SAE Aero Design Knowledge, 2021

School Name: *Dwarkadas J. Sanghvi College of Engineering*

Team Name: *DJS SKYLARK - MICRO CLASS*

Team Number: *314*

Team Members
Team Captain: Shome Vakharia

Aaryan Shah
Abhimanyu Suthar
Abhishek Malichkar
Arshish Balaporia
Aryan Ashar
Aryan Thukral
Harshal Soni
Hiral Shah

Jinay Gandhi
Joel Ponmany
Kenith Shah
Kirtan Jhaveri
Lobhas Patankar
Nainika Shah
Neel Mehta
Neil Vashani
Parv Khandelwal
Radhika Puranik
Raj Anadkat
Rishi Ghia

Roshan Sam
Sharva Potdar
Shikha Punjabi
Shlok Mandloi
Shubham Mody
Tanmay Kshire
Ved Vartak
Vighnesh Patil

STATEMENT OF COMPLIANCE

Certification of Qualification

Team Name   **DJS Skylark – MICRO CLASS**   Team Number   **314**

School   **Dwarkadas J. Sanghvi College of Engineering**

Faculty Advisor   **Prof. Shashikant Auti**

Faculty Advisor's Email   **shashikant.auti@gmail.com**

Statement of Compliance

As faculty Adviser:

SMA (Initial) I certify that the registered team members are enrolled in collegiate courses.

SMA (Initial) I certify that this team has designed and constructed the radio-controlled aircraft in the past nine (9) months with the intention to use this aircraft in the 2021 SAE Aero Design competition, without direct assistance from professional engineers, R/C model experts, and/or related professionals.

_Sm A_ (Initial) I certify that this year's Design Report has original content written by members of this year's team.

SMA (Initial) I certify that all reused content have been properly referenced and is in compliance with the University's plagiarism and reuse policies.

_SM A_ (Initial) I certify that the team has used the Aero Design inspection checklist to inspect their aircraft before arrival at Technical Inspection and that the team will present this completed checklist, signed by the Faculty Advisor or Team Captain, to the inspectors before Technical Inspection begins.

_____   25/02/2021
Signature of Faculty Advisor   Date

_____   28/02/2021
Signature of Team Captain   Date

Table of Contents

List of Symbols

C	Chord of the control surface		S1	Maximum control surface deflection
C_D	Drag coefficient of aircraft		S2	Maximum servomotor deflection
C_{Di}	Lift-induced drag coefficient		S_{TO}	Take-off Distance
C_{D0}	Zero-lift drag coefficient		T_s	Static Thrust
C_f	Skin friction drag coefficient		T_d	Dynamic Thrust
C_L	Lift coefficient of aircraft		v	Airspeed
C_M	Coefficient of pitching moment of aircraft		v_d	Dive speed
D	Drag		v_e	Exit Velocity
g	Acceleration due to Gravity		v_{gE}	Gust Velocity
k_g	Gust coefficient		W	Weight of the aircraft
L	Lift		α	Angle of attack
m	Mass of the aircraft		ρ	Density
n	Load factor		ω	Frequency
S	Wing Planform Area		Φ	Aircraft Bank Angle

List of Abbreviations

AR	Aspect Ratio		MoS	Margin of Safety
CFD	Computational Fluid Dynamics		PLA	Polylactic Acid
CG	Centre of Gravity		TMA	Tail Moment Arm
FoS	Factor of Safety		VLM	Vortex Lattice Method

List of Figures and Tables

Figure 1(a)	System Overview and Discriminators		Figure 4(a)	V-n Diagram
Table 1(b)	Subsystem Details		Table 4(b)	Landing Shock Calculations
Figure 2(a)	Schedule Summary		Figure 4(c)	Environmental Considerations
Figure 2(b)	Schedule and Cost Breakdown		Chart 5(a)	Developed Models
Table 2(c)	Risk Analysis		Figure 5(b)	Dynamic Thrust Performance
Figure 3(a)	Wing Layout		Figure 5(c)	Take-off and Climb Out Telemetry
Figure 3(b)	Fuselage Layout		Figure 5(d)	Minimum Turning Radius
Figure 3(c)	Empennage Layout		Figure 5(e)	Maximum Banking Angle
Figure 3(d)	Avionics System Layout		Figure 5(f)	Short Period and Phugoid Modes
Figure 3(e)	Time Bottleneck Analysis		Table 5(g)	Stability Response
Figure 3(f)	Planform Analysis		Table 5(h)	Lateral Stability Eigenvalues
Figure 3(g)	Aircraft Configuration Analysis		Figure 5(i)	Drag Polar Analysis
Table 3(h)	Aircraft Configuration Details		Table 5(j)	Material Selections
Figure 3(i)	Weibull Curve		Figure 5(k)	Crosswind Analysis
Figure 3(j)	Score vs Windspeed		Figure 5(l)	Composite Stress Analysis
Figure 3(k)	Delivery Box Biplane Analysis		Figure 5(m)	Weight Distribution
Figure 3(l)	C_m vs α		Table 6(a)	Servo Torque Requirements
Figure 3(m)	Motor-Propeller Combinations		Chart 7(a)	Manufacturing Process

1.0   Executive Summary
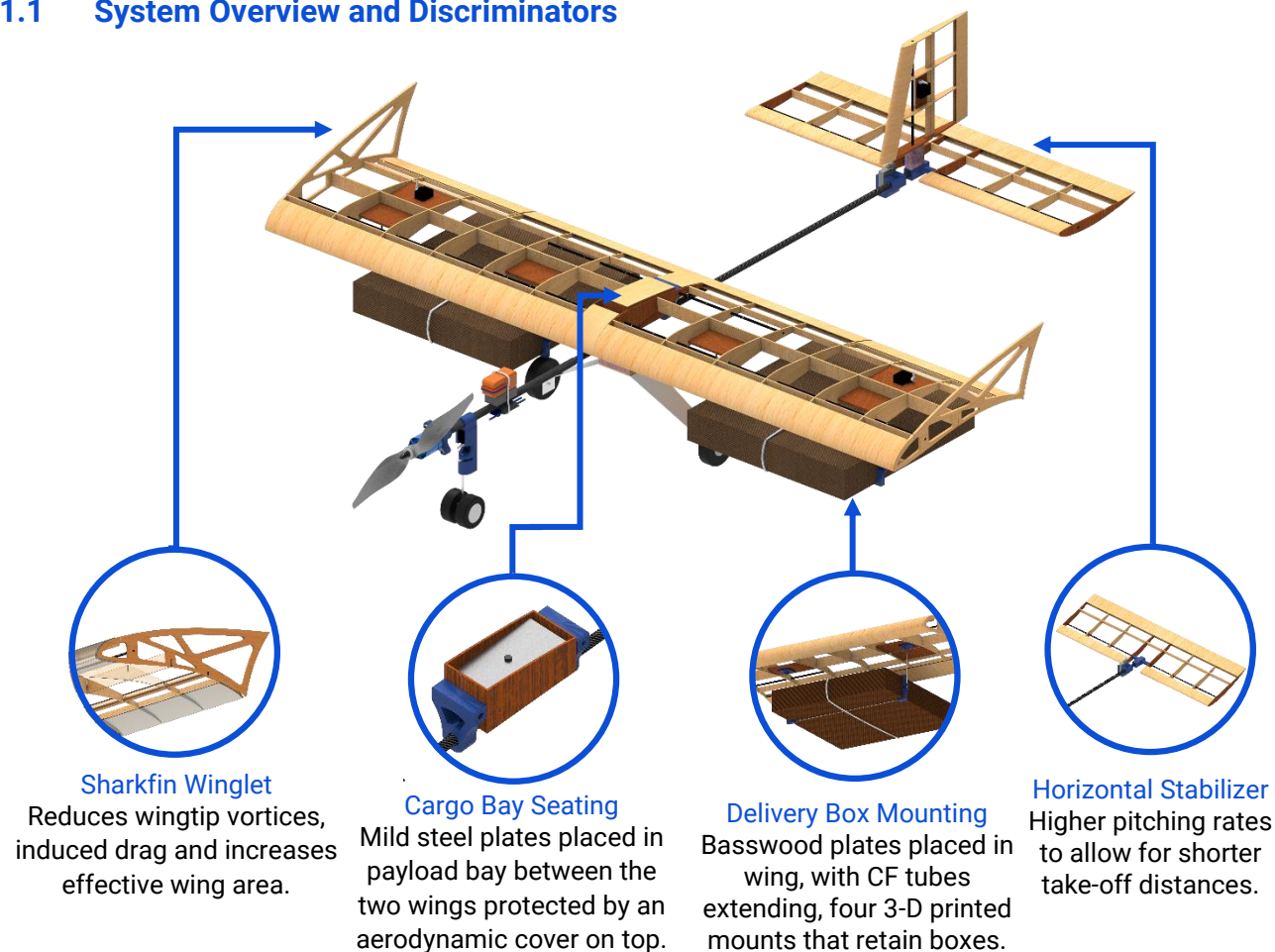
1.1   System Overview and Discriminators

Sharkfin Winglet
Reduces wingtip vortices, induced drag and increases effective wing area.

Cargo Bay Seating
Mild steel plates placed in payload bay between the two wings protected by an aerodynamic cover on top.

Delivery Box Mounting
Basswood plates placed in wing, with CF tubes extending, four 3-D printed mounts that retain boxes.

Horizontal Stabilizer
Higher pitching rates to allow for shorter take-off distances.

Figure 1(a): System Overview and Discriminators

Avionics		
Motor	**Propeller**	**Battery**
SunnySky 2820 860 KV	APC 14x7 E	Dinogy LiPo 850mAh 4S
Wings		
Airfoil	**Span**	**Planform**
S1223 RTL	48in	Rectangular
Empennage		
Horizontal Tail Airfoil	**Vertical Tail Airfoil**	**Configuration**
AH 79-100C (50%) and NACA 0009 (50%) interpolated	NACA 0009	Inverted T-Tail
Scoring Strategy		
Delivery Boxes	**Time Taken to 300 ft. (sec)**	**Payload Plates (lbs.)**
2 Large Boxes	7.2	2.65

Table 1(b): Subsystem Details

1.2   Competition Projections

The team designed the aircraft to carry 3.34 lbs. of total cargo weight, comprising 2 Large Delivery Boxes and 2.65 lbs. of Payload Plates in 7.2 seconds: achieving a projected score of 28.59 points per round and 85.77 points in total. Combining our flight scores with strong Design Report and Technical Presentation scores, we aim to place in the Top 3 Overall. We obtained these scores by performing in-depth analyses on the scoring equation to understand which parameters to optimize, followed by extensive trade studies for each component based on the results obtained from the former.

2.0   Project Management

2.1   Schedule Summary

The COVID-19 pandemic and the resulting lockdown in India heavily affected the team's schedules and ability to manufacture and test prototypes throughout the year. Work began in September after the rules were published, until which, we invested all our time in training junior members and testing new materials. We based our schedules on monthly cycles of design, testing and optimization working around our exam schedule. 4 prototypes were built and tested with each bringing into the foray a slew of improvements and optimizations.
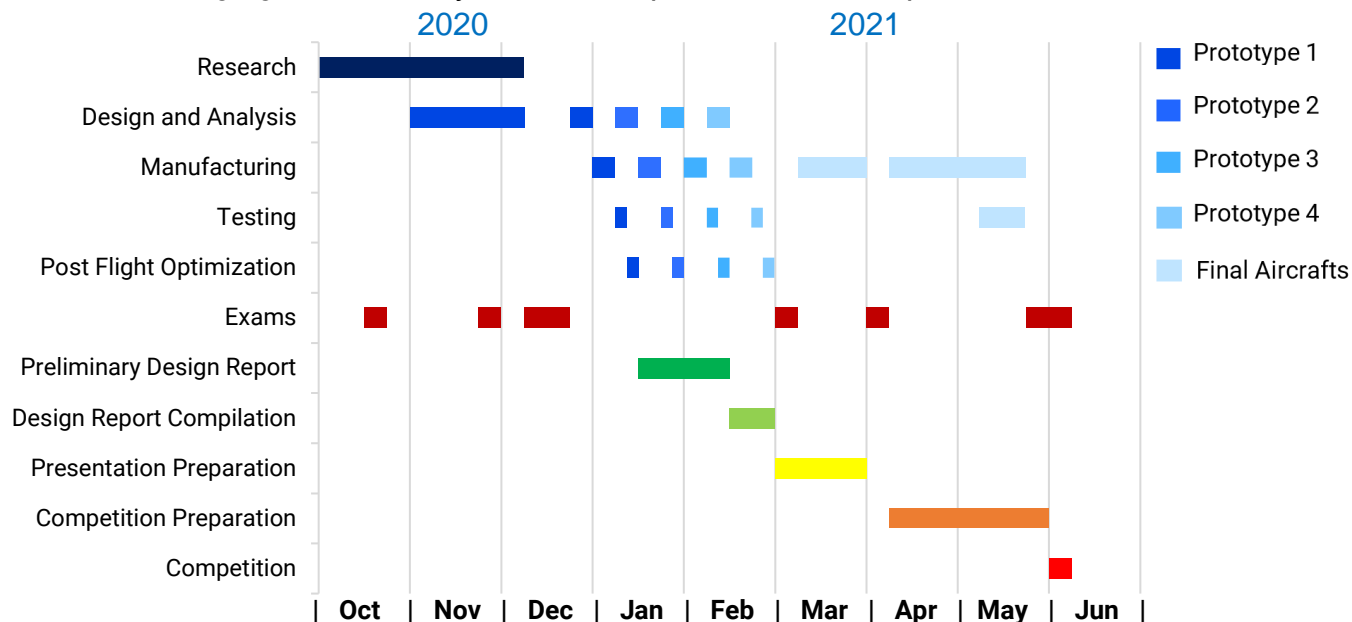

Figure 2(a): Schedule Summary

2.2   Personnel Management

Comprising of 29 students, the team was segregated into aerodynamics, structures, avionics, and marketing departments; ensuring ideas could be shared and discussed effectively inter and intra-departmentally, allowing for progress in designs for both Micro and Regular classes. Over time, Design Report and Technical Presentation groups were formed.
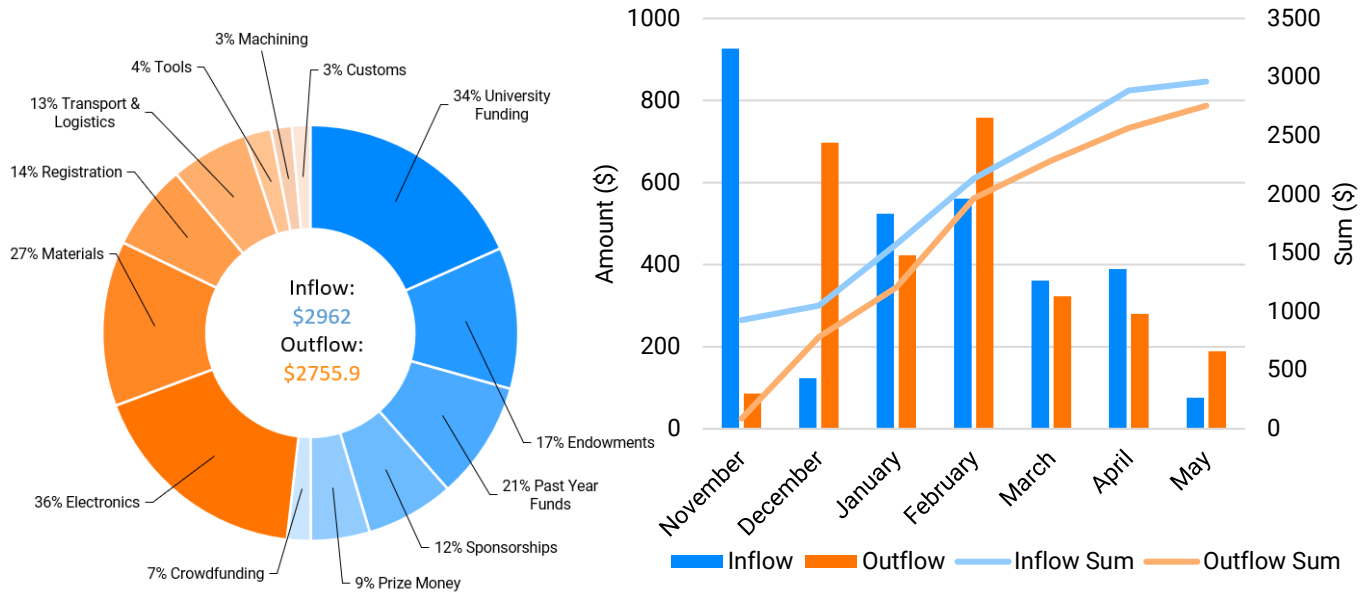
2.3   Cost Report

Figure 2(b): Schedule and Cost Breakdown

COVID-19 heavily affected the team's inflow of funds starting with delayed and reduced university funding and crowdfunding, close to no sponsorships as well as cancellation of the annual aero-modelling workshop the team conducts to raise majority of its funds annually. The outflow of funds largely comprised of electronic components, raw material procurement, manufacturing tools, registration fee and logistics. To reduce the high costs of material procurement, we contacted international wholesalers directly. Heavy customs duty, long shipping periods and product unavailability worldwide limited our options for testing avionics, which we overcame by using online tools to shortlist components before testing. **Figure 2(b)** represents how funds were managed through the year to eliminate any financial blockages in the design process and manufacturing.

2.4   Risk Analyses

Risk Factor	Probability of Occurrence	Impact	Mitigation
Crosswinds	High	High	Minimize longitudinal section area by eliminating the conventional fuselage
Wing & Tail Strikes	Low	Medium	Addition of a wingtip fence to prevent wing strikes and XPS Foam block to protect from tail strikes
Motor Mount Failure	Low	High	Use 3-D prints with high infill percentages and have the mount be easily replaceable in the case of a failure
Control Surface Failure	Medium	Medium	Combined use of other control surfaces to make the airplane glide to safety
Structural Component Failure	Low	High	Choose materials such as Carbon Fiber (CF) with a high tensile strength
Material Acquisition Delays	High	High	Spare materials and components to be reserved along with a scheduled time & personnel management
Monetary Constraints	High	High	Acquiring funds through online Crowd funding and organizing seminars

Table 2(c): Risk Analysis

3.0 Design Layout and Trades

3.1 Overall Design Features and Details

3.1.1   Wings

Airfoil Shaped Ribs
S1223-RTL with chord length 12". Made from 2mm thick balsa to reduce factor of safety and empty weight. Carbon Fiber main spars used to resist bending loads on wing.

Aileron
Covers 11.38 % of wing area for high rolling moments. Placed outside the range of influence of delivery boxes for optimal performance.

Shark-Fin Winglet
Allows for increase in effective wing area and reduction in induced drag. Assists in preventing tip-stall.
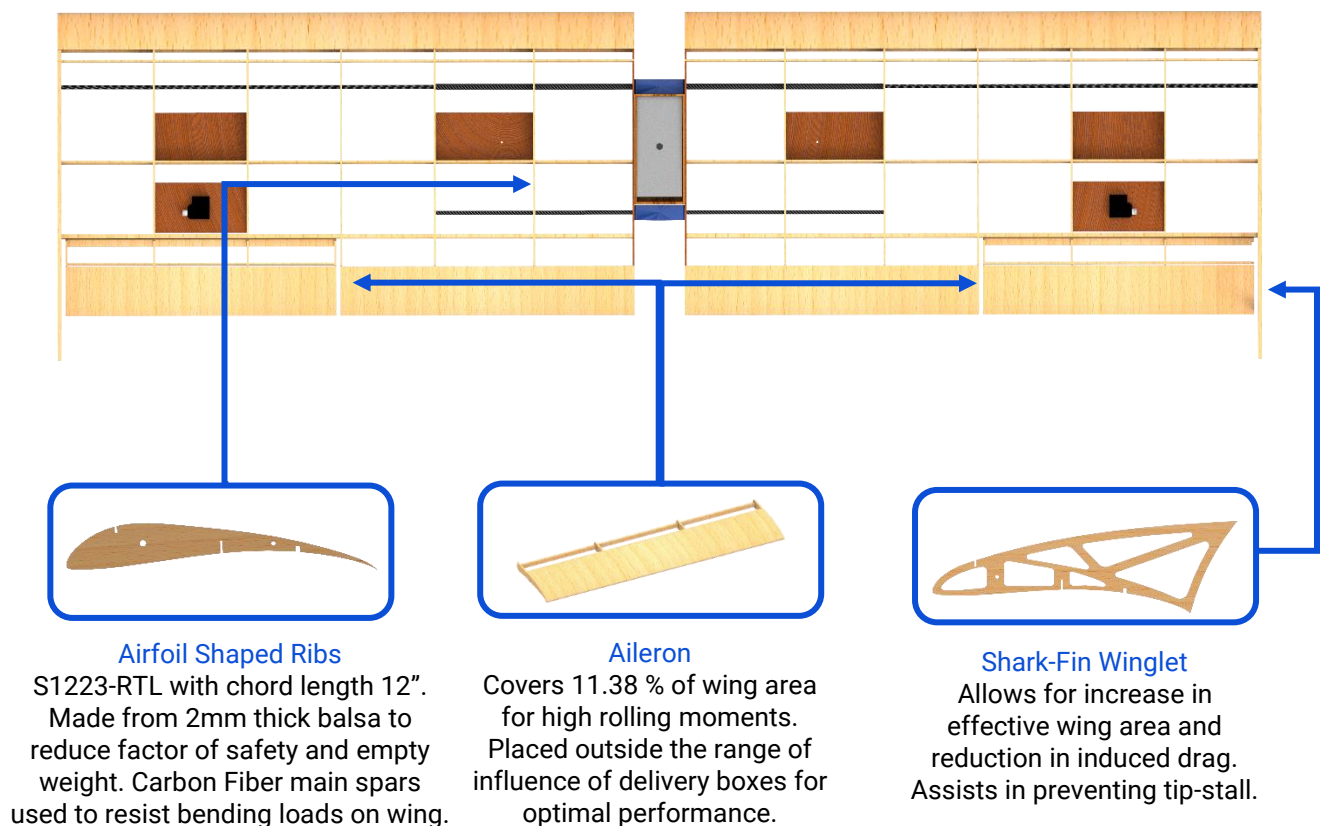
Figure 3(a): Wing Layout

The team opted for a rectangular planform choosing airfoil the S1223 RTL with the maximum permitted wingspan of 48in. The wing is made of airfoil-shaped ribs, retained in place with balsa jigs and two hollow co-axial Carbon Fiber main spars to sustain in-flight loads while maintaining a low empty weight. The wing is held in place by two 3-D printed mounts connected to a single cylindrical Carbon Fiber boom.

3.1.2 Fuselage and Landing Gear

Landing Gear
Made of a 3-D printed mount holding a single cylindrical aluminum spoke in place connected to 2 wheels to allow for effective steering. Main Landing Gear made of machined aluminum to resist landing impacts.
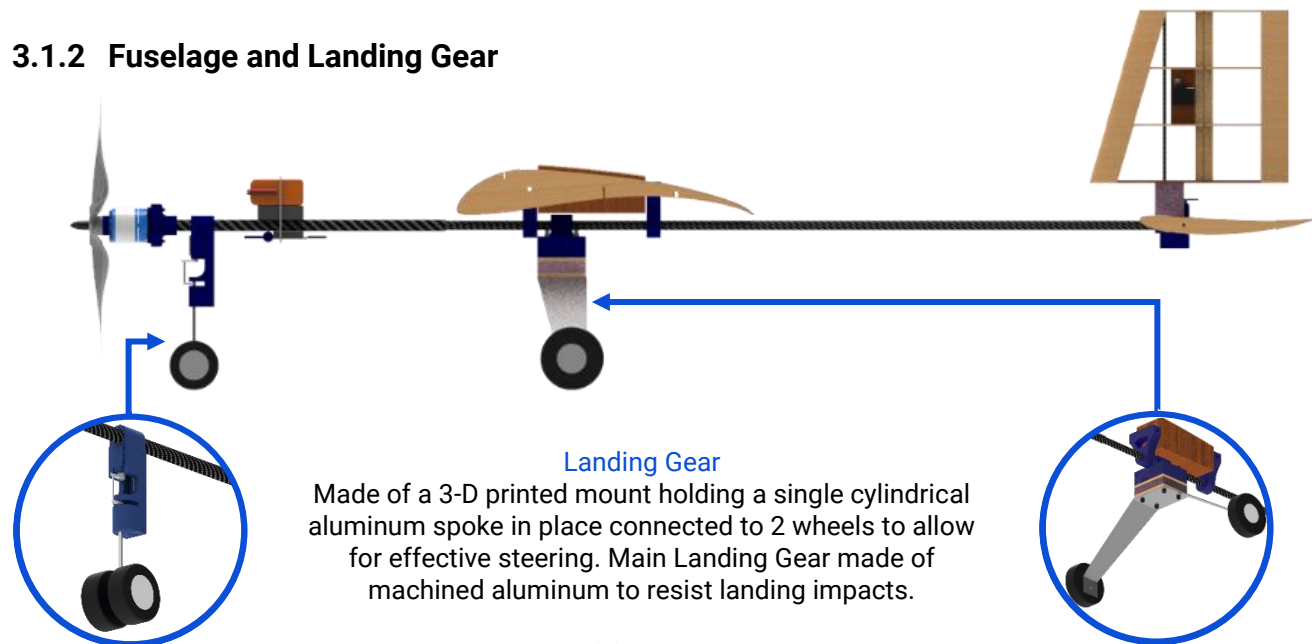
Figure 3(b): Fuselage Layout

The fuselage comprises of two co-axial CF pipes of diameters 12 and 10mm respectively connected to the motor, battery, wings, and tails using 3-D printed connectors. It is 54.2% lighter than a conventional fuselage, while reducing drag **(Section 3.2.3)** and the FoS. A tricycle landing gear (LG) is used owing to its immunity to ground looping and as it lets the tail overhang the platform, thus enabling efficient use of the 8 ft. take-off distance.

3.1.3 Delivery Boxes and Payload

The team machined 2.65 lbs. of mild steel plates (4in x 1.8in x 0.118in). They majorly influence CG and are therefore placed near the desired CG, in a cargo bay made of basswood, which is retained laterally by the wings and longitudinally by the 3-D printed wing mounts. Efficient packaging, ease of loading and machinability of steel plates were given priority, their dimensions

being derived primarily from the dimensions of the mounts. Aerodynamic covers are added between the wings, above, in front of and behind the plates to reduce drag. The boxes are retained under the wings by a rectangular structure with 3D printed mounts which facilitate connection of the structure to the wings using carbon fiber tubes.

3.1.4 Empennage

Vertical Stabilizer
NACA 0009 airfoil
of Root Chord 8"
Tip Chord 6".

Horizontal Stabilizer
AH 79-100C airfoil
of 7" chord used.

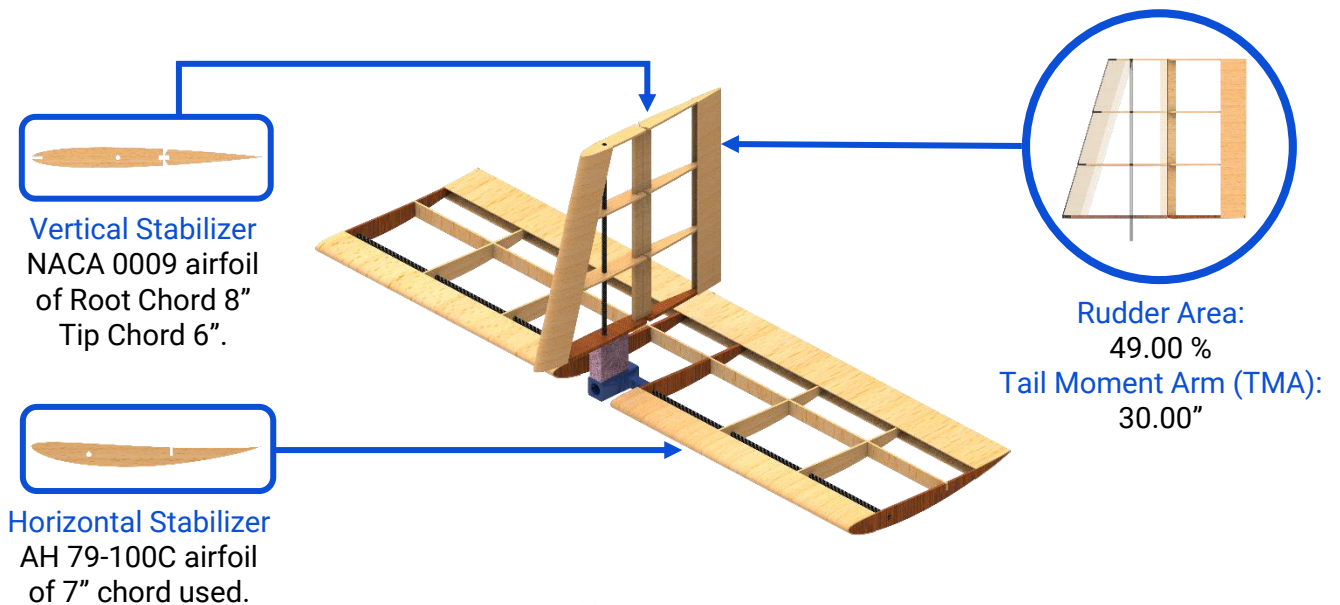Rudder Area:
49.00 %
Tail Moment Arm (TMA):
30.00"

Figure 3(c): Empennage Layout

The aircraft utilizes an inverted T-Tail configuration for its reliability while reducing empty weight by 34% as compared to a U-Tail. We decided to use the horizontal stabilizer as a control surface, giving us higher pitching moments compared to a conventional elevator arrangement. A Carbon Fiber tube was used as the primary spar for both, the vertical and horizontal stabilizers.
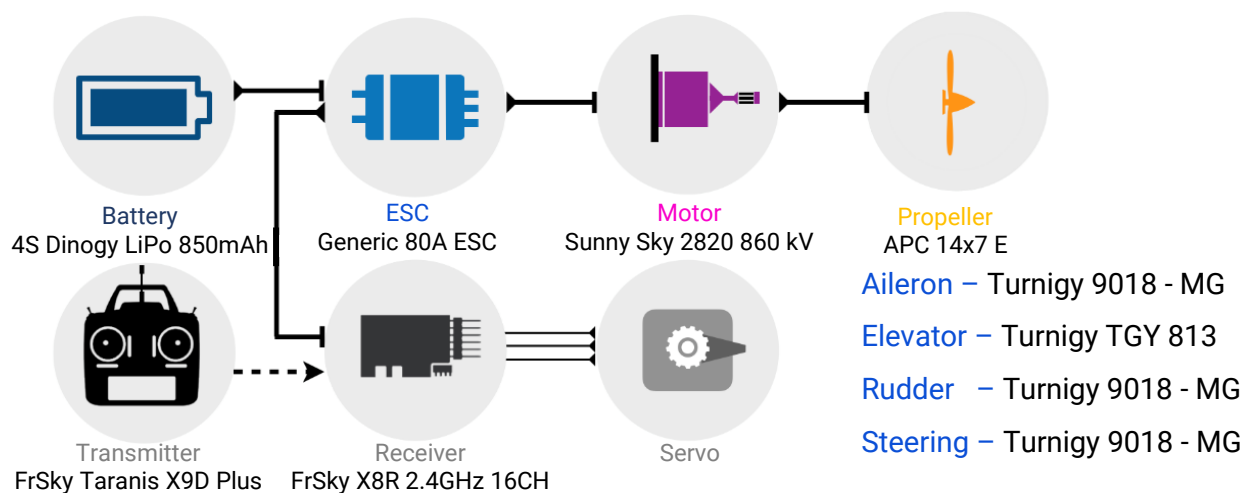
3.1.5 Avionics

Battery
4S Dinogy LiPo 850mAh

ESC
Generic 80A ESC

Motor
Sunny Sky 2820 860 kV

Propeller
APC 14x7 E

Transmitter
FrSky Taranis X9D Plus

Receiver
FrSky X8R 2.4GHz 16CH

Servo

Aileron – Turnigy 9018 - MG
Elevator – Turnigy TGY 813
Rudder   – Turnigy 9018 - MG
Steering – Turnigy 9018 - MG

Figure 3(d): Avionics System Layout

3.2   Competitive Scoring Strategy and Analyses

The new scoring equation has 3 primary variables - Payload, Delivery Boxes and Time. With the variables being interdependent, optimizing the wing planform and cargo configuration independently and combining them is not viable as each cargo configuration requires a unique wing planform to minimize time and achieve the best possible score for that configuration. Since all parameters must now be optimized simultaneously, we performed analyses observing how each factor interacts with the other.

3.2.1 Optimization and Sensitivity Analyses

The optimization goal on the scoring equation is maximizing the numerator and minimizing the denominator. Time being in the denominator with an index of 1, the score is highly sensitive to it, however, time is also the variable out of the three to be most affected by external factors such as environmental conditions and varying pilot inputs as can be seen in **Section 3.2.4**. Thus, we performed analyses on the slowest and fastest possible configurations, to understand the limits of time optimization and the threshold after which the gradient of score increase against time flattens out, as shown below.
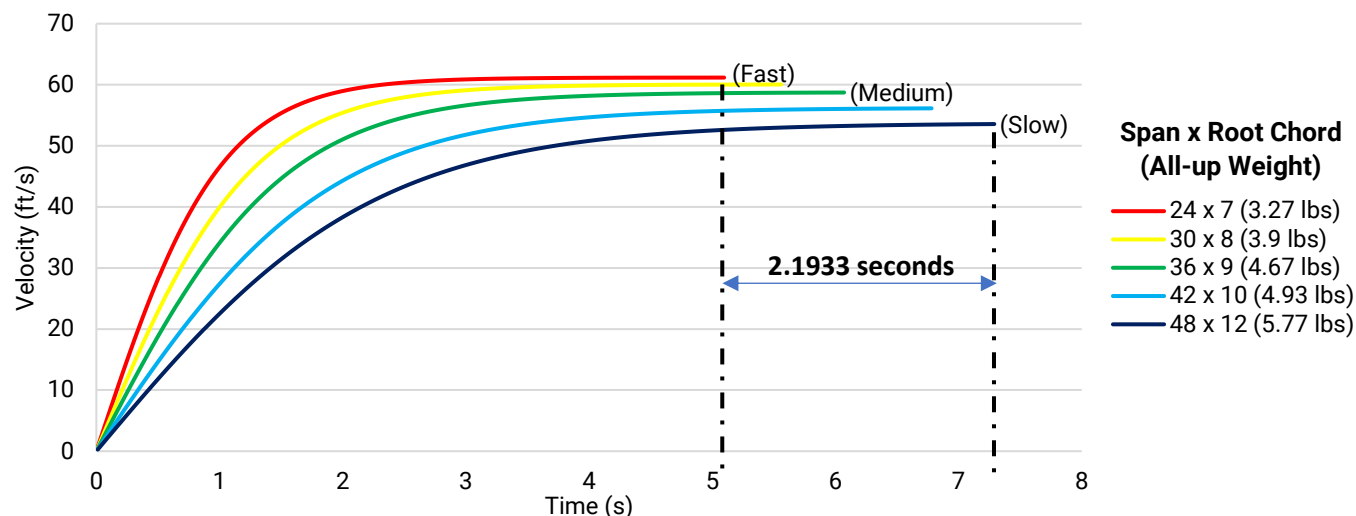

Figure 3(e): Time Bottleneck Analysis

Time optimization is limited by the propulsion system's dynamic thrust performance and pitch speeds. We performed thrust tests on over 25 Motor-Propeller combinations **(Section 3.3.5)**.

This allowed us to find the threshold beyond which time could not be reduced keeping in mind the 450W limit. We plotted the velocity versus time to 300 ft. graphs for 5 different wing planforms representing the entire domain, each having its optimal motor-propeller combination. Planforms were chosen based on their lift and drag characteristics, with the 24" wingspan representing a light, fast time-based scoring strategy aircraft, and the 48" wingspan to represent a relatively heavier, slower payload-based strategy. The fastest time observed is 5.0969s, which itself does not include Empennage, Boom, Mounting and most importantly Delivery Box Drag. Thus, the time cannot be reduced beyond this threshold for the given range of inputs, with only a difference of 2.19s between the slowest (heaviest) and fastest (lightest) configurations.
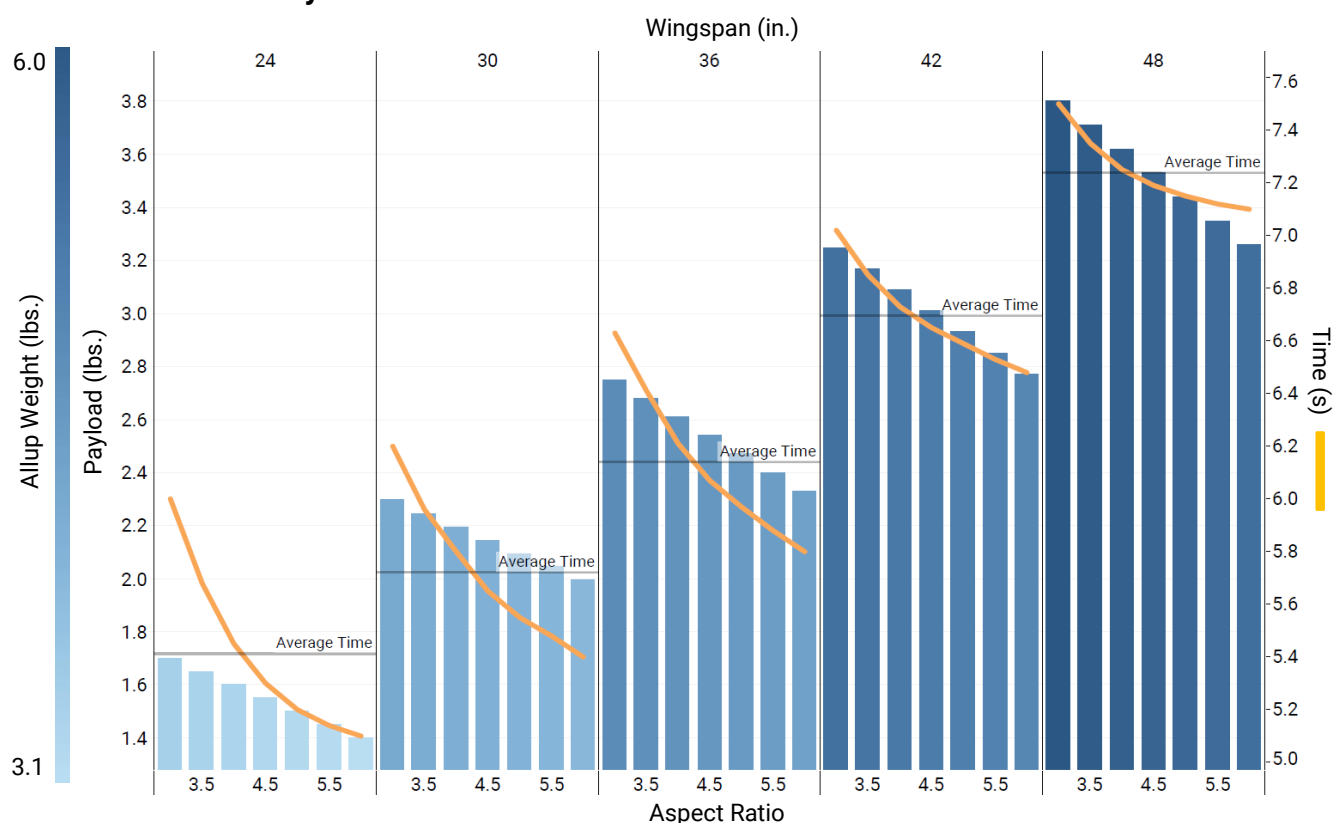
3.2.2 Planform Analysis

Figure 3(f): Planform Analysis

We curated a database of multiple airfoils to maximize lift, airfoil efficiency, and stall angle, while minimizing drag. Of these, S1223RTL was found to perform the best overall. Subsequently, we ran the Tornado VLM Solver in MATLAB performing an exhaustive search in the domain on over

500 wing planforms with varying dimensions of Root Chords 6"-15", Tip Chords 6"-15", Spans 24"-48", and Aspect Ratios 3-6. The top 10% configurations of each span were shortlisted, and high mesh Solidworks CFD Analyses were run on them for more accurate results. We factored in the empty weight increase for wingspans by calculating the quantity of balsa used; evaluating the mass properties provided by our CADs. Lift and Drag values obtained were used as inputs. to our score, time and take off distance calculator (**Section 5.2**). Delivery boxes influence the drag and lift of the aircraft, thus we performed planform analysis on the wings without any delivery boxes present. We analyzed the effect of wing planforms with differing spans and aspect ratios on the payload lifted and time taken. The slope of time flattens with increasing aspect ratio and the gradient of time flattens with increasing wingspan.

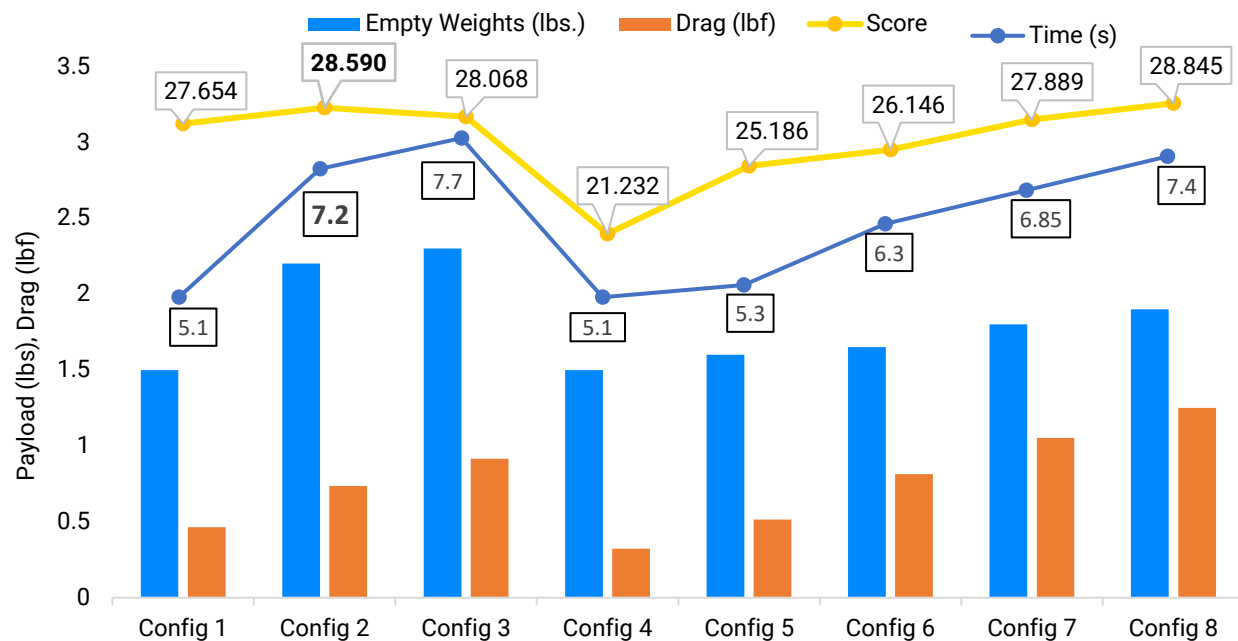### 3.2.3 Aircraft Configuration Analysis

Figure 3(g): Aircraft Configuration Analysis

Parameters	Configurations							
	Config 1	**Config 2**	**Config 3**	**Config 4**	**Config 5**	**Config 6**	**Config 7**	**Config 8**
No. of Large Boxes	1	2	3	0	0	0	0	0
No. of Small Boxes	0	0	0	1	2	3	4	5
Span (in)	35	48	48	24	28	36	44	48
Root Chord (in)	12	12	12	8	8	10	10	10
Drag (lbf)	0.46	0.74	0.91	0.32	0.51	0.81	1.05	1.25

*The above configuration numbers shall be used for reference throughout the report.

Table 3(h): Aircraft Configuration Details

We built upon the exhaustive search mentioned in the previous section, mapping each wing planform against each cargo configuration, factoring in the variation in empty weight and drag with changes in Wing Planforms and different box mountings. Time, empty weight and take off distance reduction being paramount; the team eliminated the conventional fuselage and stacking delivery boxes within it; for its inability to optimally satisfy the above criterion. Mixed delivery box strategies were eliminated on similar lines, seeing as it would lead to two different kinds of mountings, redundancy and thus an increase in empty weight and drag. We categorized these configurations into three sections: Slow, Medium, and Fast fliers as classified in **Figure 3(e)**. We further shortlisted the best scoring configurations in each category and plotted them against their Empty Weights, Overall Drag and Time taken.

3.2.4 Time Sensitivity Analysis

The team plotted a Weibull Distribution for windspeeds in the first week of June taking into account data from the last 5 years. The mean windspeed is found to be 4.52 ft/s, with the most probable windspeed being 3.37 ft/s. We plotted the three best configurations from **Section 3.2.3** with their scores against the full range of possible wind speeds. Configuration 2 is found to perform optimally within 2 standard deviations, making it more resistant to external factors such as headwinds and varying pilot inputs.
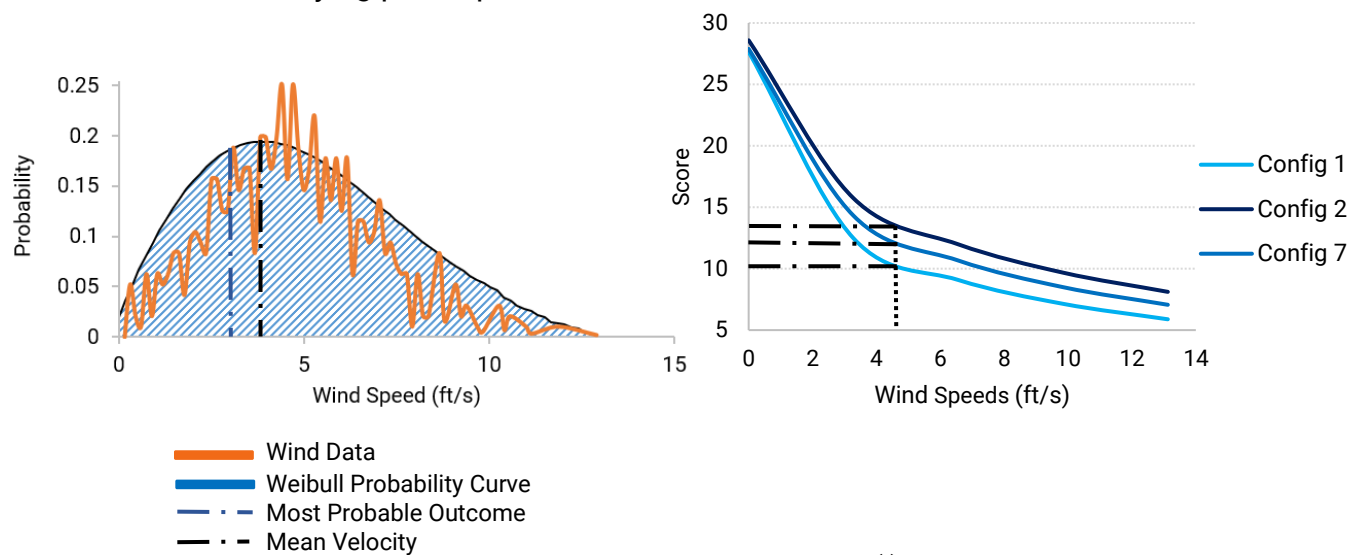

Figure 3(i): Weibull Curve

Figure 3(j): Score vs Wind Speed

3.2.5 Delivery Box Trade Analyses

All above configurations come with an associated drag penalty due to the boxes' large rectangular frontal areas. When made to sit on their largest side, both boxes have equal longitudinal section and frontal areas (24 in^2). In contrast, the large box's slender shape and height of 2" reduces wake region, along with having four times the bottom area of the small box allowing it to have a significant aerodynamic advantage. With a large box mounted on either side of the boom under the wings as in Configuration 2, a bi-plane like effect is generated **(Section 3.3.1)** with the large boxes performing as exaggerated flat-plate airfoils providing lift increase by 23% assisting with takeoff in 0.65 ft less, partially offsetting its drag penalty. The final aircraft configuration selected is a wing planform of span 48" and chord 12", 2 Large Delivery Boxes, 2.65 lbs. of Payload Plates lifted scoring 28.59 points per round.

3.3 Design Derivations

3.3.1 Wings

The team built 4 prototypes, testing high-lift devices, materials, planforms, and mountings. The first prototype was built with a 48x14in rectangular wing planform maximizing payload lifted at the cost of time. The second prototype in contrast was built to minimize empty weight, drag, and time with a 36x12in wing planform. Consequently, in accordance with the competitive scoring strategy, third prototype's wing planform of 48x12in was found to be the most optimal selection. We built upon the same planform in the 4th prototype, reducing the FoS to reduce weight. The chord length of 12" allows us to mount large boxes underneath the wing without significantly hampering downwash. We chose a rectangular planform as tapering the wing led to only an 8% reduction in drag which in turn caused a drop in score. With the boxes generating a biplane like effect, we optimized it's mounting location by running CFD analyses varying the Gap, Stagger and Decalage, the results for which are plotted below.
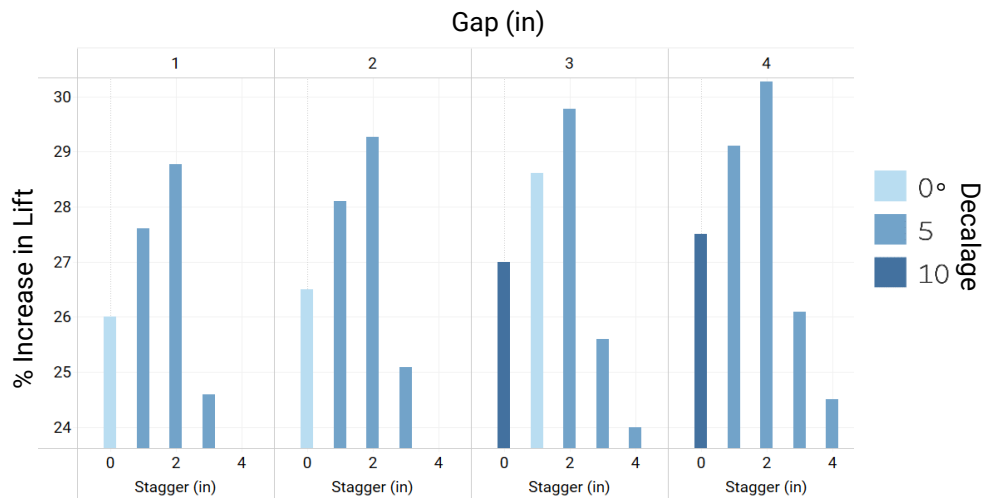
Figure 3(k): Delivery Box Biplane Analysis

We ran CFD Analyses in order to optimize box placements adopting a biplane analogy. The selected configuration is a gap of 3 ", Stagger of 1.5" and no decalage. 4" gap was rejected for its lack of ground clearance.

3.3.2 Fuselage

The first prototype was built with a conventional fuselage to sustain heavy landing shocks. A twin Carbon Fiber tail boom was added to increase strength and reduce weight in lieu of a conventional tail section. This fuselage was eliminated in later iterations by virtue of drag, weight and FoS reductions. The primary dimensions of the Carbon Fiber Tail Boom were derived by satisfying the required TMA, CG position, Avionics, and Payload Plate placement. The fuselage longitudinal section area was reduced by 37% over the first iteration to improve crosswind performance. We chose top loading of payload plates onto a basswood plate between the wings as it provided fast and easy loading without the need for additional structures.

3.3.3 Vertical Tail

We initially used a U Tail to avoid the Fuselage wake region; later combatted by eliminating the fuselage entirely. Thus, we chose a conventional tail for its low empty weight. We sized the tail by calculating the required tail volume coefficient (0.047), by analyzing crosswinds at the Lakeland **(Section 5.4.2)**. NACA 0009 was selected for its low drag at 0° angle of attack.
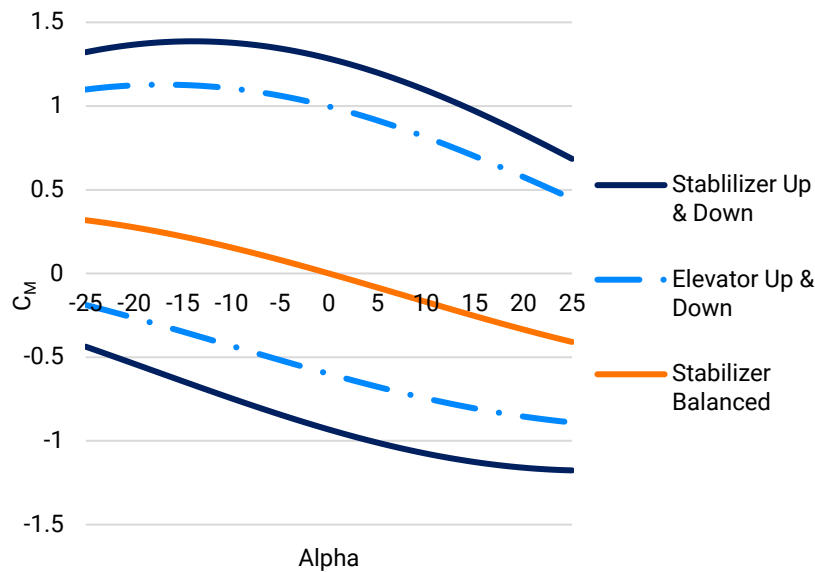
3.3.4 Horizontal Tail

Figure 3(l): C_M vs Alpha

To achieve a balanced and positively stable empty and loaded CG position, the team calculated and balanced the resulting moments of each force acting on the aircraft including Lift, Drag, Thrust, Weight at CG, and Tail force. The tail sizing and inverted asymmetrical airfoil [AH 79-100 C (50%) and NACA 0009 (50%) interpolated] were chosen to achieve the required level of pitching moment.
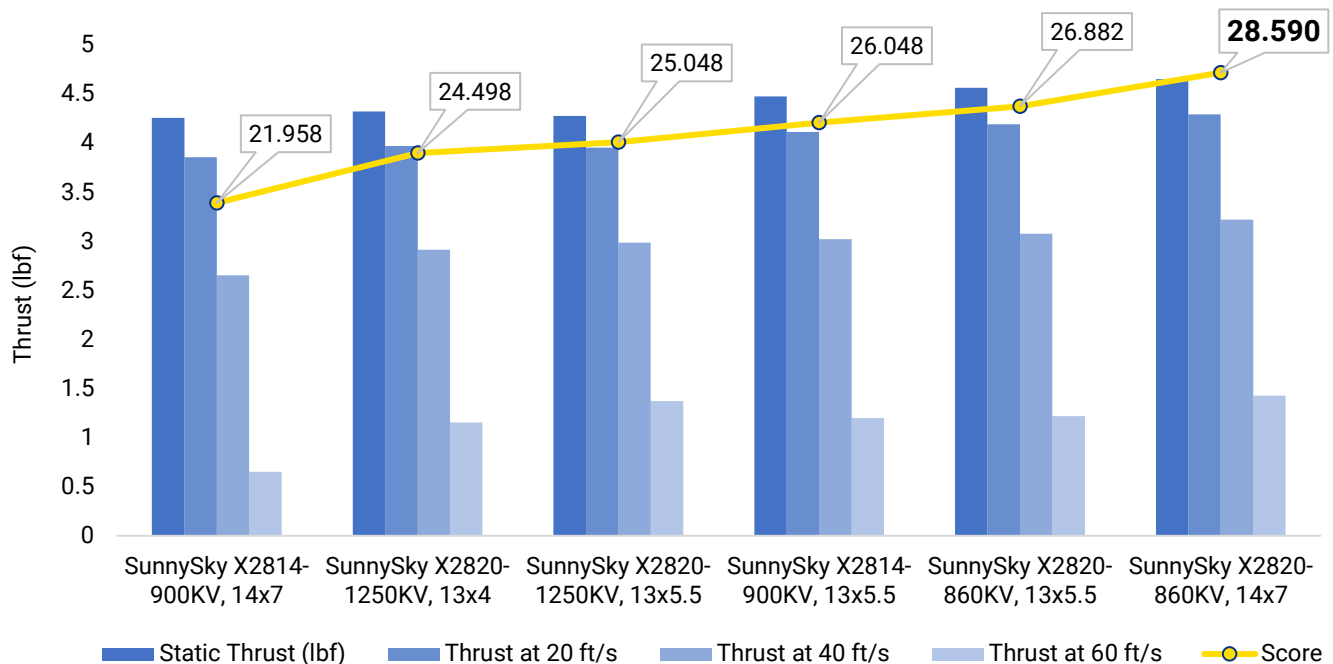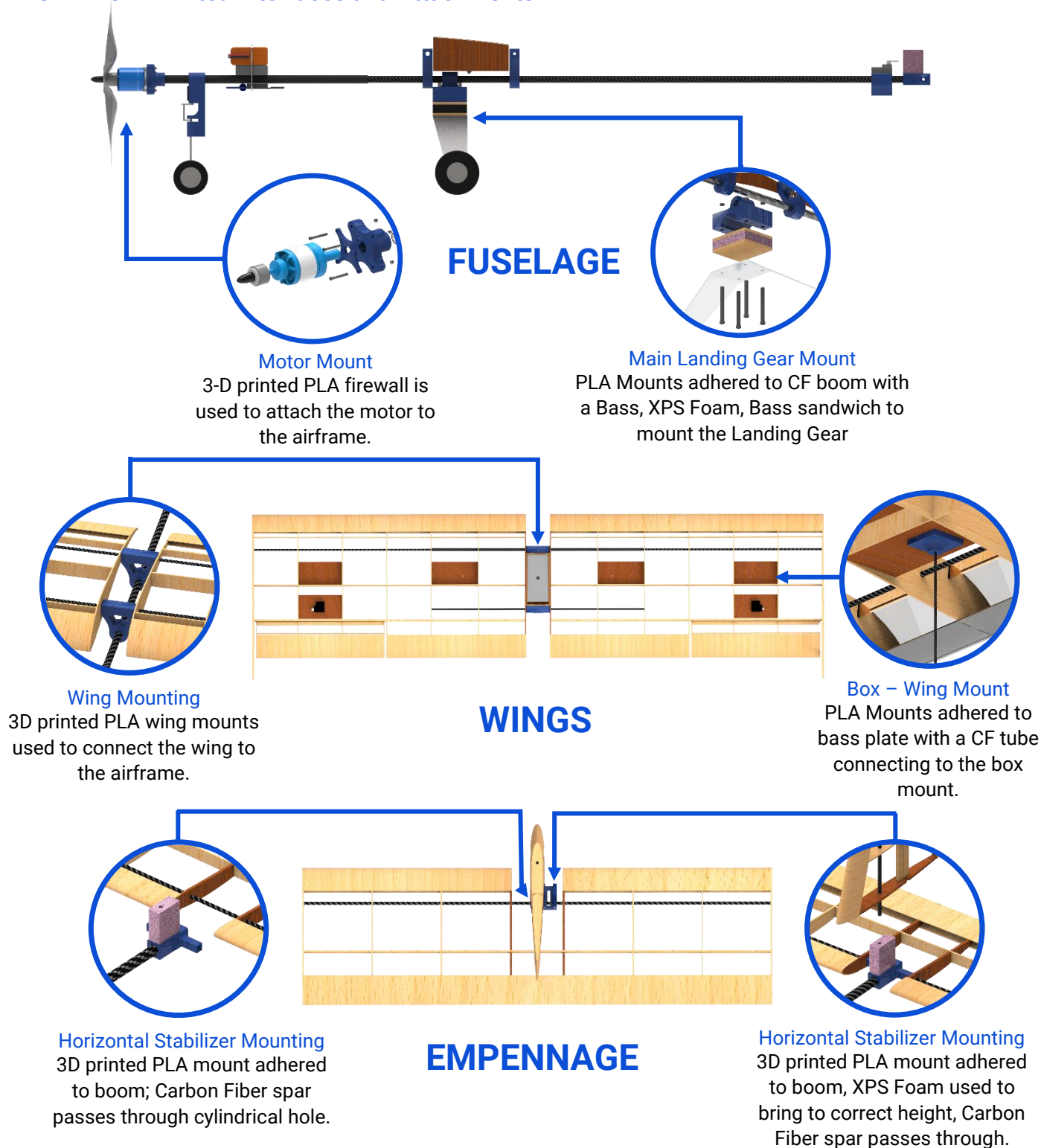
3.3.5 Avionics:

Figure 3(m): Motor-Propeller Combinations

The selection of motor and propeller was based on dynamic performance analysis for various flight conditions of take-off, turning and cruising. Better dynamic performance was prioritized based on the bottleneck analysis performed earlier. Later, the same hypothesis was reinforced

by extensive flight tests, showing motor-propeller combinations with better dynamic performance outscoring their counterparts by virtue of higher speeds and reduced time. The required torque at the control surface hinge was calculated as mentioned in Appendix A, at the dive speed of the aircraft.

3.4   3-D Printed Interfaces and Attachments

FUSELAGE

Motor Mount
3-D printed PLA firewall is used to attach the motor to the airframe.

Main Landing Gear Mount
PLA Mounts adhered to CF boom with a Bass, XPS Foam, Bass sandwich to mount the Landing Gear

Wing Mounting
3D printed PLA wing mounts used to connect the wing to the airframe.

WINGS

Box – Wing Mount
PLA Mounts adhered to bass plate with a CF tube connecting to the box mount.

Horizontal Stabilizer Mounting
3D printed PLA mount adhered to boom; Carbon Fiber spar passes through cylindrical hole.

EMPENNAGE

Horizontal Stabilizer Mounting
3D printed PLA mount adhered to boom, XPS Foam used to bring to correct height, Carbon Fiber spar passes through.

4.0   Loads, Environments and Assumptions

4.1   Design Load Derivations
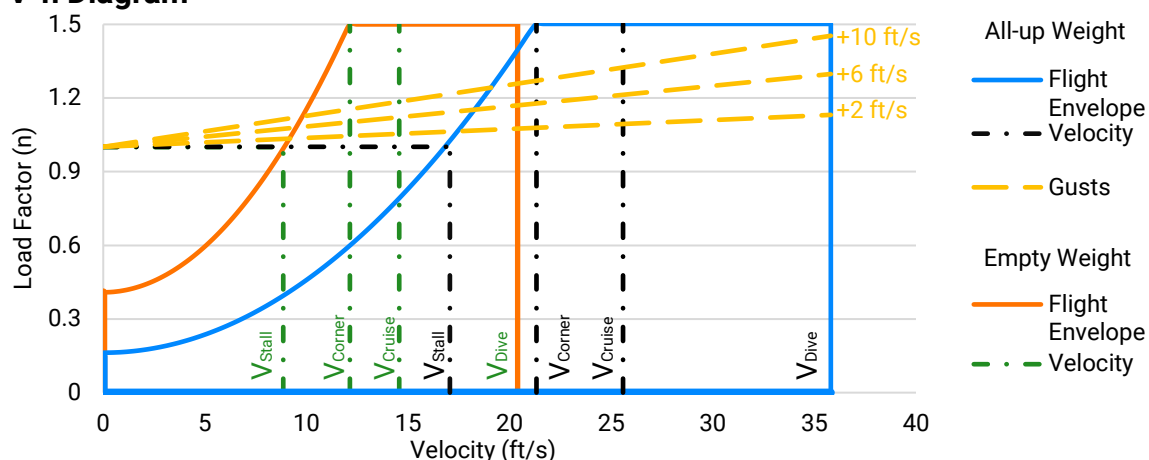
4.1.1 V-n Diagram

Figure 4(a): V-n Diagram

The V-n diagram is generated for empty and all-up weight of the aircraft. The load factor is non-zero when the aircraft is stationary due to the effect of propwash. Gust velocities of 2ft/s, 6ft/s and 10ft/s were also considered for the all-up weight load case.

4.1.2 Landing Shocks

Glideslope	Sink Rate (ft/s)	Impact Loading (lbf)
3°	0.861	23.8497
5°	1.434	39.7218
10°	2.856	79.1112

Table 4(b): Landing Shock Calculation

The team calculated the impact loading on the airframe during touchdown for glideslopes of 3, 5 and 10° by calculating change in momentum and normal force. We used telemetry data to derive the former and calculate approach velocity. We recorded the median impact time as 0.2 seconds from multiple flight tests. The 3-D printed main landing gear mount was designed with a FoS of 1.632 keeping these loads in mind.

4.2   Environmental Considerations

We calculated the scores for Mumbai and Lakeland over a period of a month (February for Mumbai, June for Lakeland) which were derived from the density altitudes, taking into account

various environmental factors such as temperature, pressure, relative humidity, dew point and altitude during the days of the competition as well as our testing period. We also took into account differing values of rolling resistance at Mumbai and Lakeland. The highest score obtained in Lakeland is 28.16 points with a decrease in score by 1.511% compared to Mumbai.
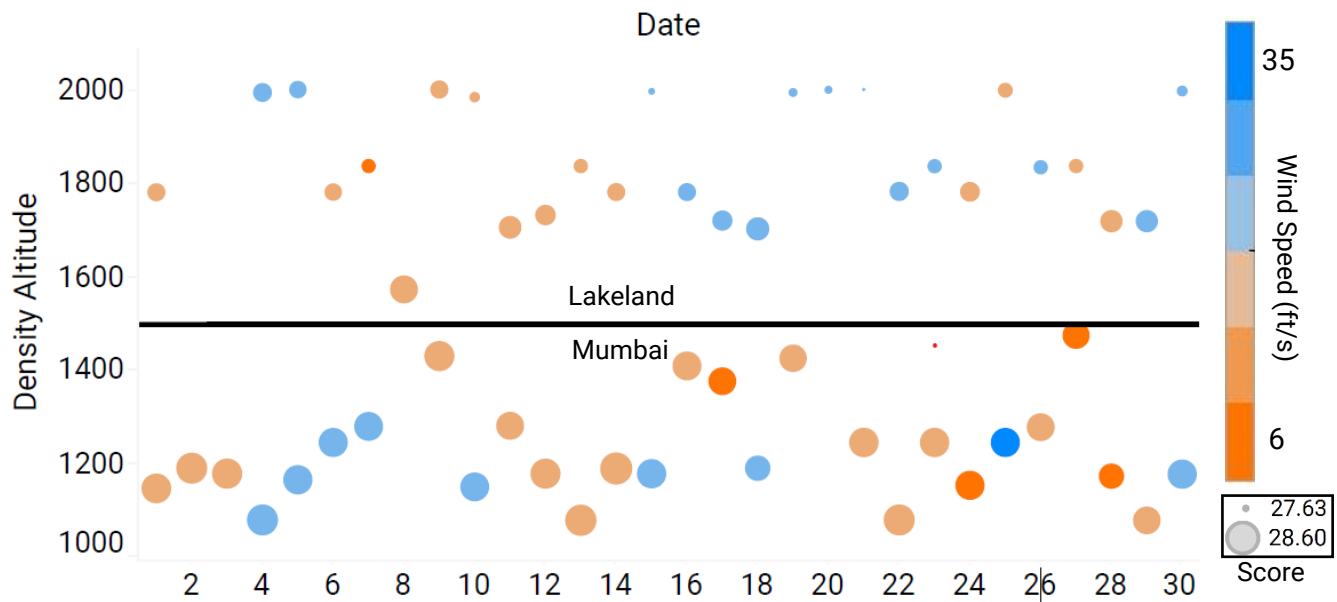

Figure 4(c): Environmental Considerations

5.0　　Analyses

5.1　　Analytical Tools

5.1.1　Solidworks and XFLR5

The team used Solidworks for CFD and Finite Element Analysis (FEA) over aerodynamic surfaces and load bearing components, respectively. We used topology optimization techniques to achieve the highest overall strength to weight ratio and provide insight into system level structural inadequacies. Solidworks was also used for accurate balancing of masses and CG. We used XFLR5 to interpolate airfoils and to export their polars. It was also used for obtaining and analyzing static and dynamic stability eigenvalues.

5.1.2 Tableau & Microsoft Excel

Used to generate detailed and efficient graphs and plots with varying scores, wingspan, cargo configurations, aspect ratios and payload showing how we optimized those parameters.

5.1.3 MATLAB and Python

We used MATLAB Module Tornado VLM to analyse wing planforms. We used Global Optimization Toolbox by MathWorks to optimize system variables using advanced techniques of genetic optimization to find the global maxima with score as the fitness value.
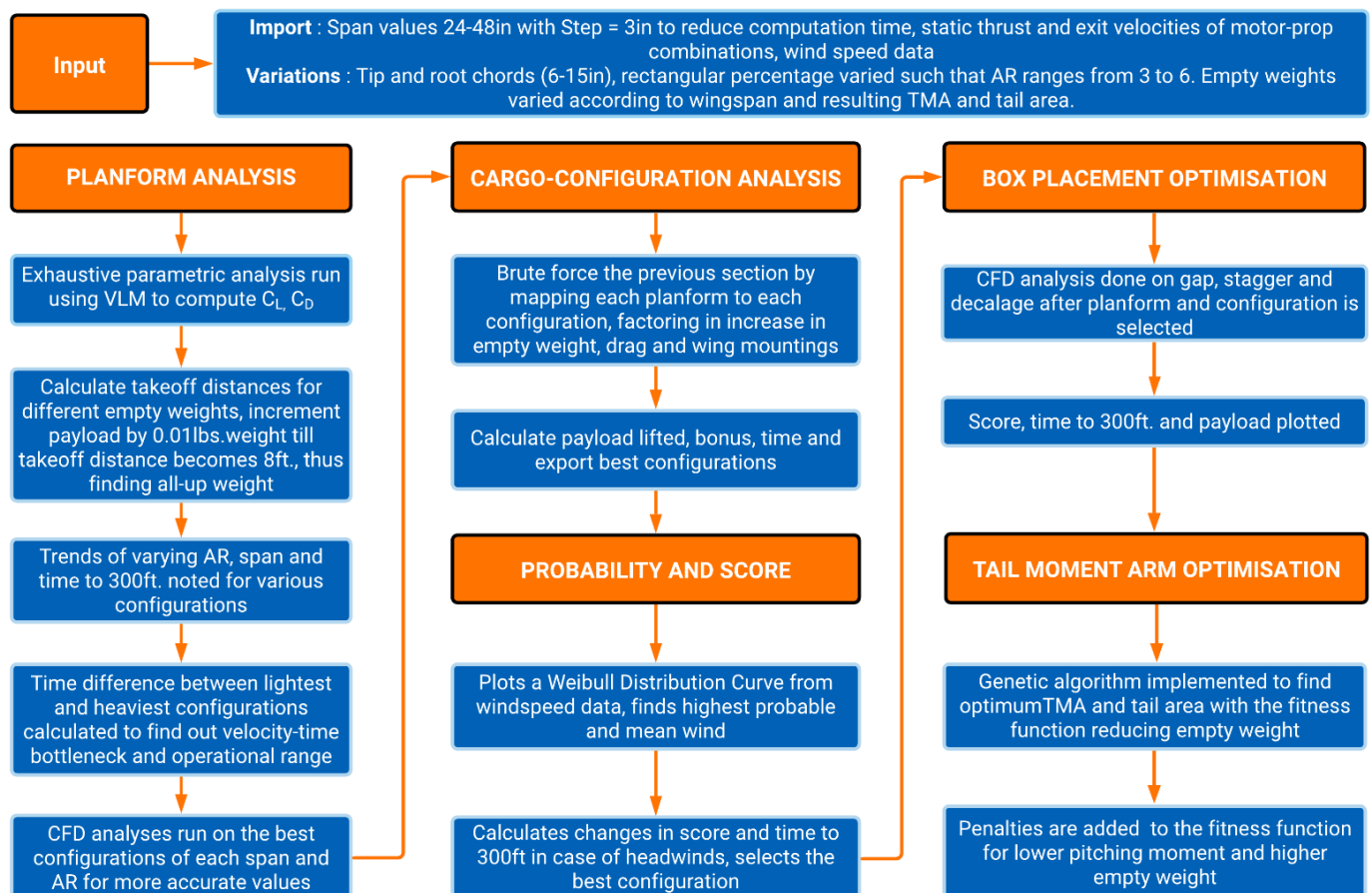
5.2 Developed Models

Input

Import : Span values 24-48in with Step = 3in to reduce computation time, static thrust and exit velocities of motor-prop combinations, wind speed data
Variations : Tip and root chords (6-15in), rectangular percentage varied such that AR ranges from 3 to 6. Empty weights varied according to wingspan and resulting TMA and tail area.

PLANFORM ANALYSIS

Exhaustive parametric analysis run using VLM to compute C_L, C_D

Calculate takeoff distances for different empty weights, increment payload by 0.01lbs.weight till takeoff distance becomes 8ft., thus finding all-up weight

Trends of varying AR, span and time to 300ft. noted for various configurations

Time difference between lightest and heaviest configurations calculated to find out velocity-time bottleneck and operational range

CFD analyses run on the best configurations of each span and AR for more accurate values

CARGO-CONFIGURATION ANALYSIS

Brute force the previous section by mapping each planform to each configuration, factoring in increase in empty weight, drag and wing mountings

Calculate payload lifted, bonus, time and export best configurations

PROBABILITY AND SCORE

Plots a Weibull Distribution Curve from windspeed data, finds highest probable and mean wind

Calculates changes in score and time to 300ft in case of headwinds, selects the best configuration

BOX PLACEMENT OPTIMISATION

CFD analysis done on gap, stagger and decalage after planform and configuration is selected

Score, time to 300ft. and payload plotted

TAIL MOMENT ARM OPTIMISATION

Genetic algorithm implemented to find optimumTMA and tail area with the fitness function reducing empty weight

Penalties are added to the fitness function for lower pitching moment and higher empty weight

Chart 5(a): Developed Models

5.3   Performance Analyses

5.3.1   Dynamic Thrust

We analyzed the dynamic thrust characteristics of various motor propeller combinations **(Section 3.3.5)**, as described in **Section 6.0**. **Figure 5(b)** compares three best combinations showing payload lifted against take-off distance. We prioritized dynamic thrust over high static thrust allowing for flight in high degrees of headwinds.
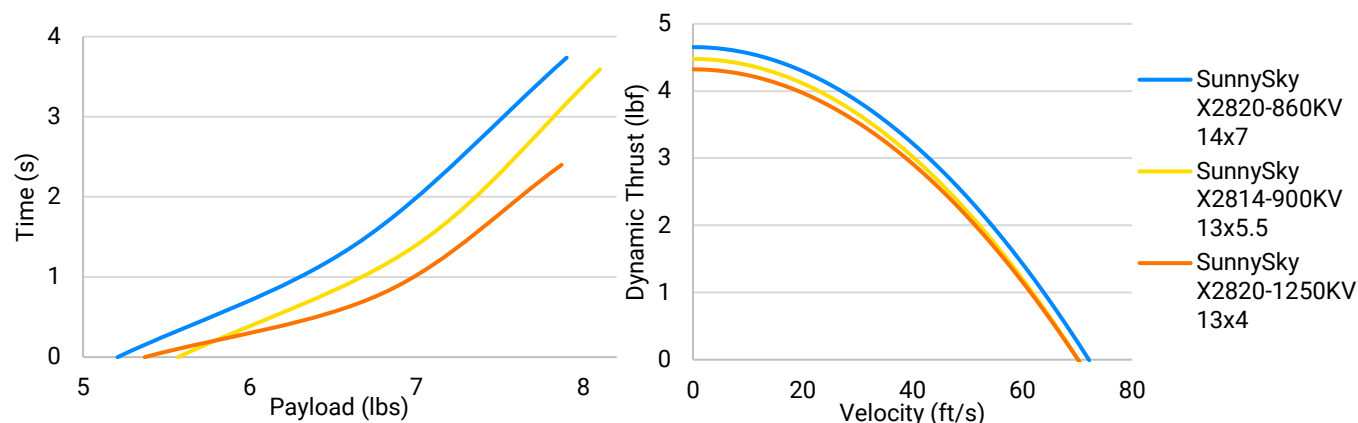
Figure 5(b): Dynamic Thrust Performance

5.3.2   Take-off and Climb Out Performance

We incorporated the equations governing take-off in our score calculator, running simulations for each iteration of our aircraft. Plotted below are the trajectories of our 4 prototypes derived from telemetry obtained after empirical testing. The 4th prototype attained take-off velocity quicker, rotated more while pitching up and gained altitude with relative ease as compared to earlier iterations. Relevant velocities and climb rates have been indicated.
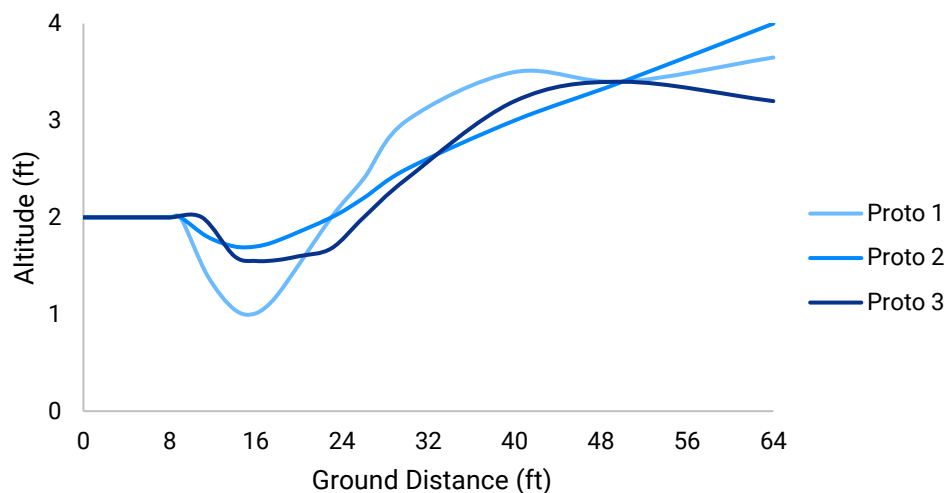
Figure 5(c): Take-off and Climb-out Telemetry

5.3.3　Flight and Maneuver Performance
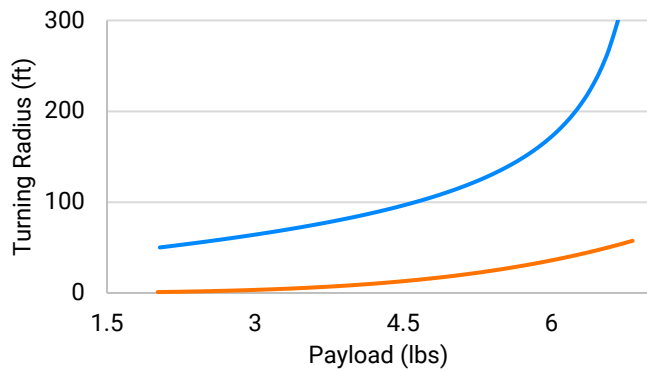
Figure 5(d): Minimum Turning Radius
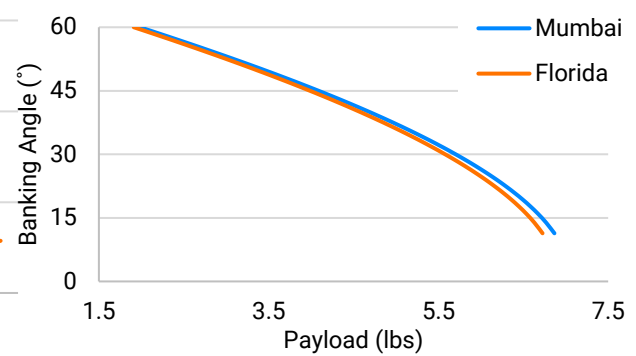
Figure 5(e): Maximum Banking Angle

The team calculated the maximum banking angles and turning radii for various load factors and velocities; by resolving the forces acting on the free-body diagram of the aircraft. The graphs represent variation in these factors depending on air densities at their respective locations.

5.3.4　Static and Dynamic Stability

The negative slope of Inverted AH 79-100C airfoil (**Figure 3(b)**) indicates that the aircraft is statically stable. The neutral point is 19.65" from the aircraft datum and the static margin is 12.5% of Mean Aerodynamic Chord.
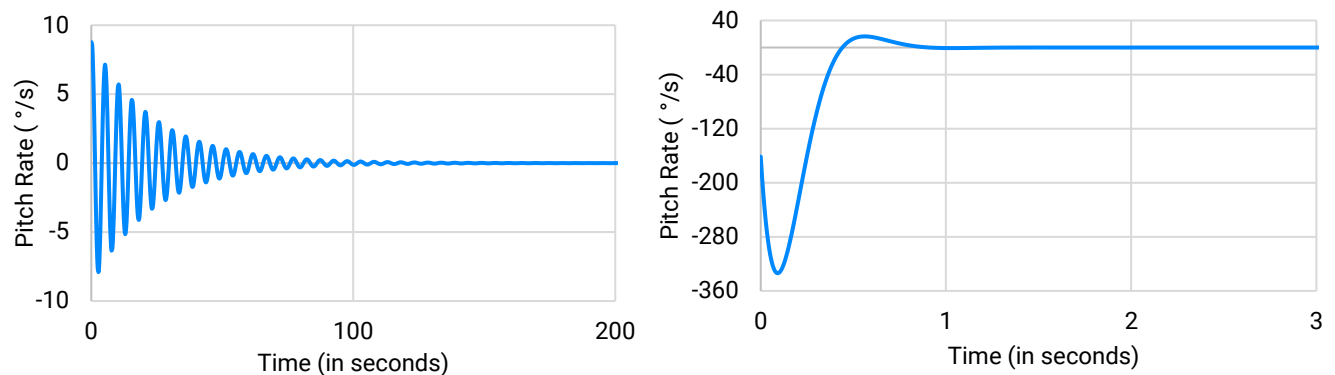
Figure 5(f): Short Period and Phugoid Modes

Oscillating Aircraft Dynamic Response		
Aircraft Motion	**Damping Factor**	**Oscillation Time (seconds)**
Short Period (Longitudinal)	0.725	0.765
Phugoid (Longitudinal)	0.031	5.586
Dutch Roll (Lateral)	0.492	1.441
Non-oscillating Aircraft Dynamic Response		
Roll Dampening (Lateral)	Tau: 0.01	Dampening Time: 0.16 seconds
Spiral Instability (Lateral)	Pilot Response Time: 1.75 seconds	Pitch Rate at Response Time: 75.62 °/s

Table 5(g): Stability Response

| Roll Dampening	-99.31927	Dutch Roll	-2.14626+3.79747i	Spiral Instability	0.7081

Table 5(h): Lateral Stability Eigenvalues

5.3.5 Aircraft Performance Prediction

The plots were generated by resolving forces and integrating the differential equation on MATLAB considering parameters like predicted headwind of 2 ft/s, rolling drag, inertia, dynamic thrust, and variation in lift and drag characteristics due to box mountings under the wings. The predicted performance was plotted for maximum payload of 2.65 lbs. and 2 large boxes.

5.3.6 Drag Polar Analysis
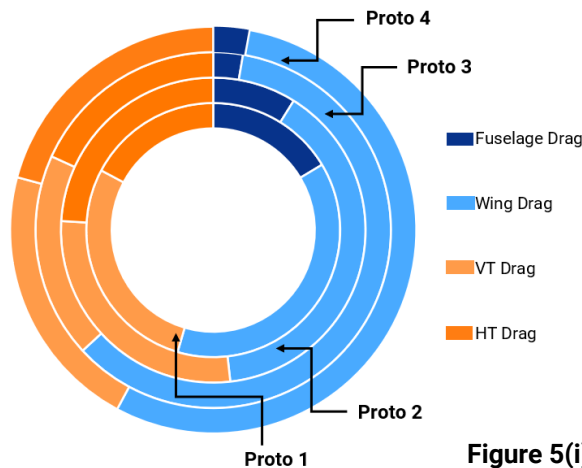
The team tabulated the percentage drag contributions of major components of the aircraft over four prototype designs, as shown here. A significant decrease in the drag of the fuselage with the second prototype.

Figure 5(i): Drag Polar Analysis

5.4 Structural Analyses

5.4.1 Critical Margins

Material	Component/Condition	Max Stress Induced (PSI)	Max Allowed Stress (PSI)	FoS
Balsa	Wing Airfoils	1214.26	1914.5	1.577
Basswood	Payload Mount during cruise	1627.38	2164.1	1.330
	Payload Mount while turning	1718.48	2164.1	1.259
Carbon Fiber	Tail Boom during cruise	5898.27	18606.89	3.155
	Tail Boom while turning	6509.56	18606.89	2.858
PLA	3D printed Attachments during cruise	5181.2	8777.25	1.694
	3D printed Attachments while turning	5622.61	8777.25	1.561

Table 5(j): Material Selection

5.4.2 Applied Loads and Material Selection

1) Tail Force Analysis

The team analyzed rudder performance under crosswind conditions by developing a mathematical model where rudder forces were measured by varying crosswind intensity during flight. It was found that the rudder becomes ineffective at 24.37 ft/s. Since Lakeland, FL has a maximum wind speed of 9.2 ft/s, the rudder will perform at 62% effectiveness.
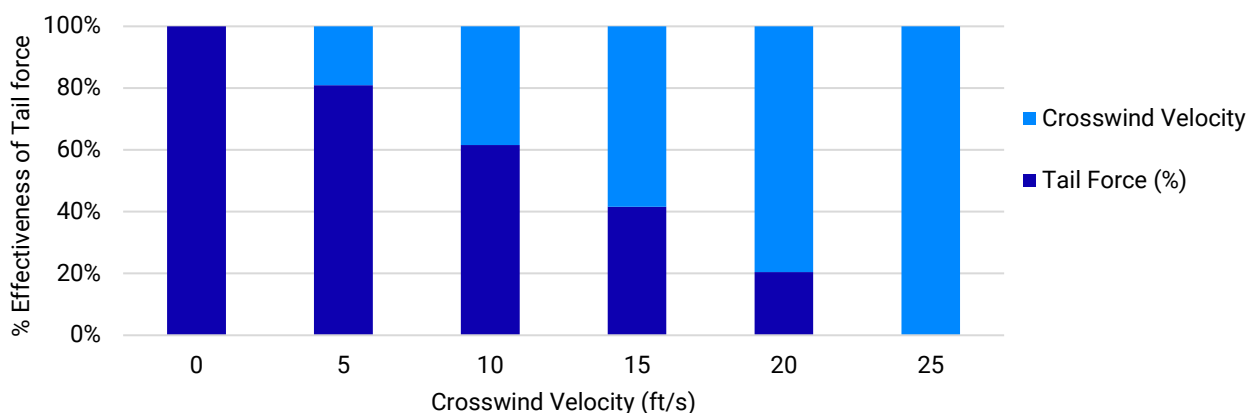
Figure 5(k): Tail Force Analysis
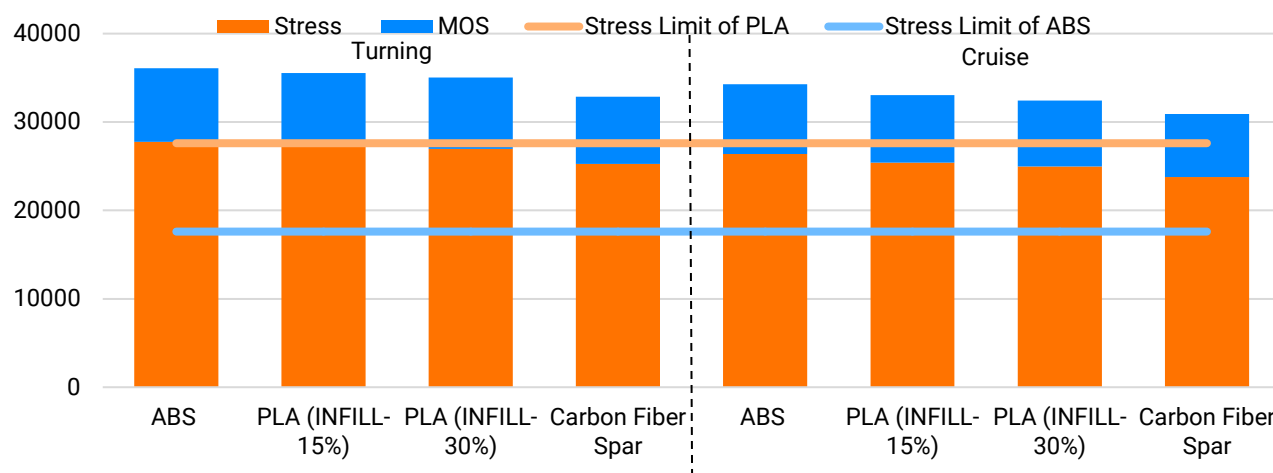
2)   Material Selection

Figure 5(l): Composite Stress Analysis

We selected a hollow carbon fiber tail boom for it's high strength to weight ratio (S/W) Ratio and ability to resist bending forces. Balsa was used in the wing and tail sub-assemblies for its low density and high S/W ratio. We used basswood at regions of concentrated loads, i.e., near the landing gears, wing, and tail junctions. PLA 3-D printed mounts were used at junctions and interfaces for ease of manufacturing, and ability to select the optimal infill densities.

3)   Mass Properties & Balance

A.   Centre of Gravity

Based on our calculations and pilot inputs, the aircraft was designed with the CG **2.33"** in front of the Neutral Point ensuring static stability. The main landing gear was placed near the CG to aid in equal weight distribution and prevent excessive loading on the nose landing gear.
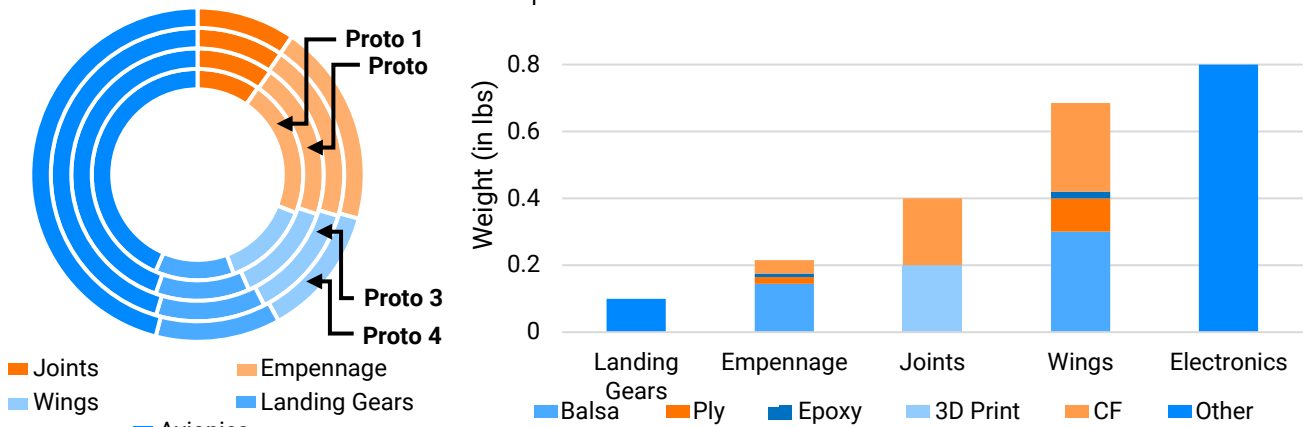
B.   Weight Distribution

Figure 5(m): Weight Distribution

6.0   Sub-Assembly Tests and Integration

6.1   Propulsion System Testing

The team shortlisted motors of kV rating 860, 900 and 1250 for testing, after comparing static thrust data from eCalc, limiting them to 450W. The dynamic thrust performance was evaluated using data sheets from APC propellers; motor-propeller options were further narrowed down.

6.2   Servo Testing

Component	Servomotor	Rated Torque (oz-in)	Control Surface Deflection	Torque Required (oz-in)
Aileron	Turnigy 9018 - MG	34.718	25°	4
Elevator	Turnigy 813	124.86	25°	47.3
Rudder	Turnigy 9018 - MG	34.718	25°	22.6
Nose Landing Gear	Turnigy 9018 - MG	34.718	25°	30.1

Table 6(a): Servo Torque Requirements

6.3   Materials and Loads Testing

We perfomed Universal Testing Machine tests on longerons, wing spar cross-sections, alternative materials and structures to identify ultimate and shear stress values. Structural loading at critical junctions was calculated to design structural members.

6.4   Flight Testing

We tested various design configurations equipped with RPM and GPS sensors, accelerometer, Pitot tube and altimeter to gather telemetry data. We conducted flights with an incremental weight build-up strategy, with the maximum lifting capacity judged from pilot feedback.
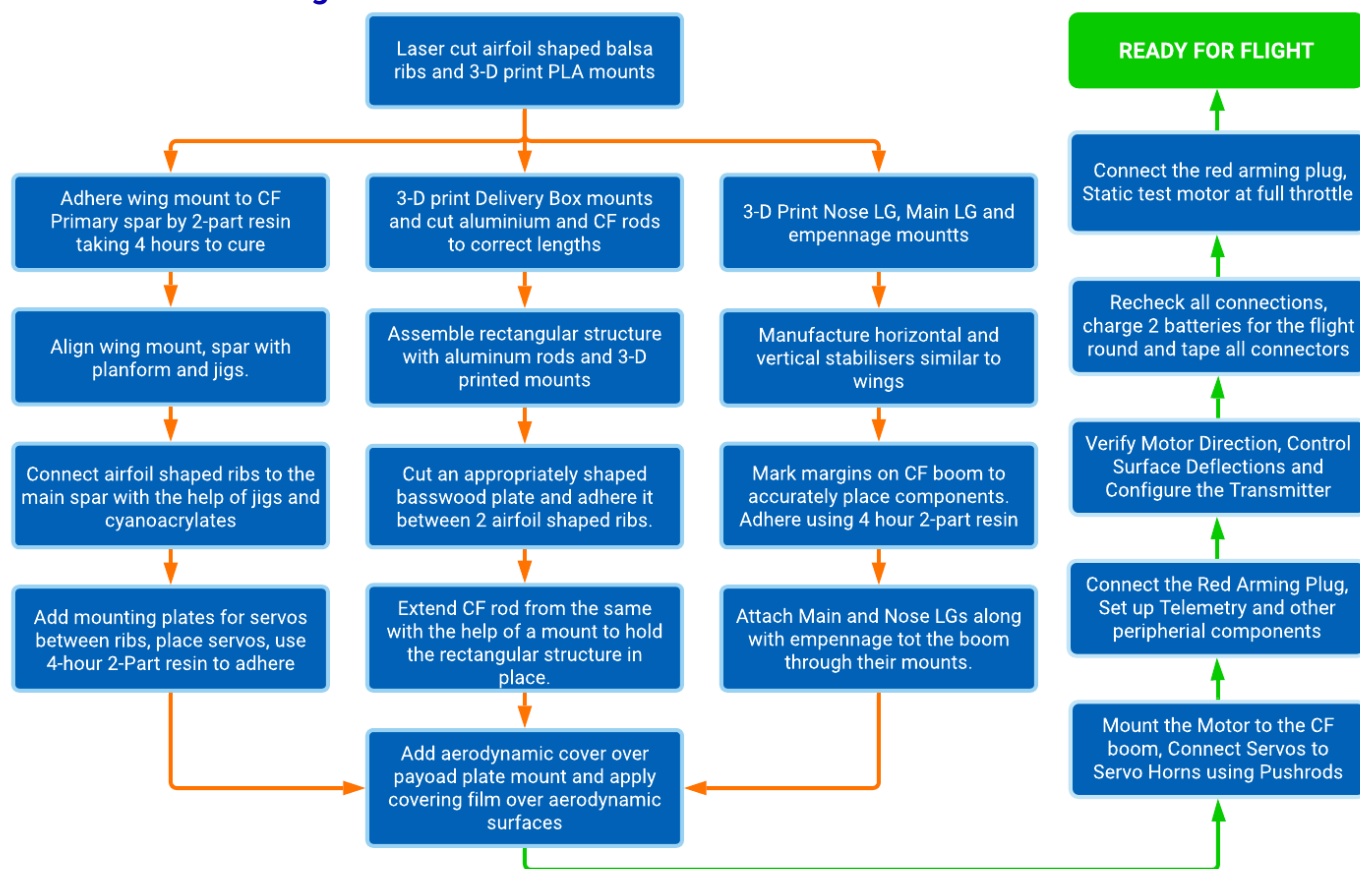
7.0   Manufacturing

Chart 7(a): Manufacturing Process

8.0   Conclusion

The designed aircraft can carry 2.65 lbs. of payload plates to 300 ft. in 7.2 seconds while carrying 2 large delivery boxes with the unique combinations of materials used ensuring structural soundness and extensive empirical testing backing our calculations. With circumstances like these, we consider ourselves fortunate to be participating this year, and expect to be competitive at SAE Aero Design Validation, 2021.

References:

1. Anderson, John D., "Introduction to Flight: Its Engineering and History.

2. Nicolai, Leland M. and Grant Carichner., "Aircraft Design"

3. Sadraey, Mohammad H., "Aircraft Design: A Systems Engineering Approach"

4. Team 024, DJS Skylark - Micro Class Design Report, SAE Aero Design East, 2020.

Appendix A – Backup Calculations

Takeoff Equation: (SECTION 5.3.2)

$$S_{To} = \frac{1}{2B} \ln \left| \frac{A}{A - Bv^2} \right| \quad ; \quad \text{Where,} \quad A = \left(\frac{T_s}{W} - \mu \right) \quad ; \quad B = \frac{g}{\omega} \left[\frac{1}{2} \rho S (C_D - \mu C_L) + \propto \right] \quad ; \quad \propto = 0.11126$$

Thrust Equations: (SECTION 3.3.5)

$$T_d = T_s - \propto v^2 \quad ; \quad \text{When } T_d = 0, \quad T_s = \propto v_e^2 \; , \quad \propto = \frac{T_s}{\left(\frac{RPM_{motor}}{60} \times pitch_{propeller} \times 0.0254 \right)^2}$$

Time: (SECTION xxx)

$$t_2 - t_1 = \frac{1}{2\sqrt{MN}} \left\{ \left[\ln \frac{\sqrt{M} + V_2\sqrt{N}}{\sqrt{M} - V_2\sqrt{N}} \right] - \left[\ln \frac{\sqrt{M} + V_1\sqrt{N}}{\sqrt{M} - V_1\sqrt{N}} \right] \right\} \quad ; \text{Where,} \quad M = \left(\frac{T_s}{w} \right) \; N = \left[\frac{g}{\omega} \left\{ \frac{1}{2} \rho S C_D + \alpha \right\} \right]$$

Where, t_2, t_1 = final and initial time and V_2, V_1 = final and initial velocity

Turning Radius Calculations: (SECTION 5.3.3)

$$\text{Radius} = \frac{mv^2}{L \sin\phi} \quad ; \quad \text{Banking Angle } (\phi) = \cos^{-1} \left(\frac{W}{L} \right)$$

Servo Torque Calculations: (SECTION 6.2)

Servo Torque Required
$$= (8.5 \times 10^{-6}) \frac{C^2 \times v_d^2 \times \text{control surface span} \times \sin^2(S_1)}{\cos(S_1) \times \tan(S_2)} \times \frac{\text{control horn height}}{\text{servo arm length}}$$

Aircraft Corner Speed (V*): (SECTION 4.4.1)　　**Gust Induced Load factor: (SECTION 4.4.1)**

$$V^* = \sqrt{\frac{2n_{max}mg}{\rho S C_{L_{max}}}} \qquad\qquad n = 1 + \frac{k_g v_{gE} v_E \alpha \rho S}{2mg}$$

Drag Polar: (SECTION 5.3.6)

$$C_D = C_{D0} + C_{Di} \; ; \quad C_{Di} = C_L^2 / (\pi \times AR \times e) \quad ; \quad C_{D0} = C_{D0(fuse)} + C_{D0(wing)} + C_{D0(Hstab)} + C_{D0(Vstab)}$$

$$C_{Dminimum(surface)} = C_{f(surface)} \times \text{Form Factor}_{(surface)} \times \frac{\text{wetted area}}{\text{reference area}} \quad ; \quad \text{Where, } e = \text{Efficiency Factor}$$

Climb Out: (SECTION 5.3.2)

$$\theta = \cos^{-1} \left(\frac{0.5\rho C_L S v^2}{mg} \right) \quad ; \quad v_y = v_x \tan\theta \quad ; \quad v = \left(v_x^2 + v_y^2 \right)^{0.5}$$

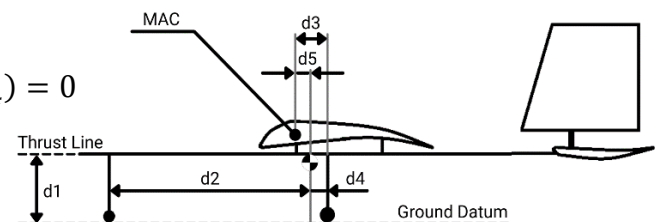v_y = velocity of aircraft in y direction; v_x = velocity of aircraft in x direction; θ = climb angle

Moment Equations: (SECTION 5.3.4)

On-ground　　$T_s d_1 - W d_2 = 0$

Take-off　　　$T_d d_1 - L d_3 + W d_4 - L_{T_1}(TMA - d_4) = 0$

In flight　　　$L_w \times d_5 = L_{T_2} \times TMA$

Where,　　　L_{T1}, L_{T2} = Tail force during take-off and in flight, respectively.
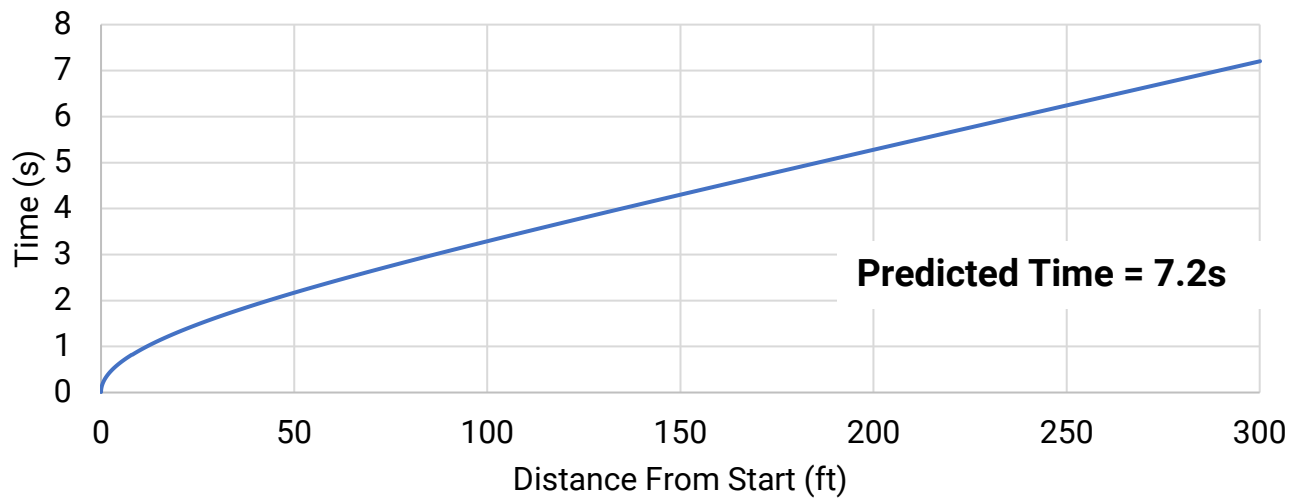
Appendix B – Technical Data Sheet

Aircraft Performance Prediction (Micro Class)
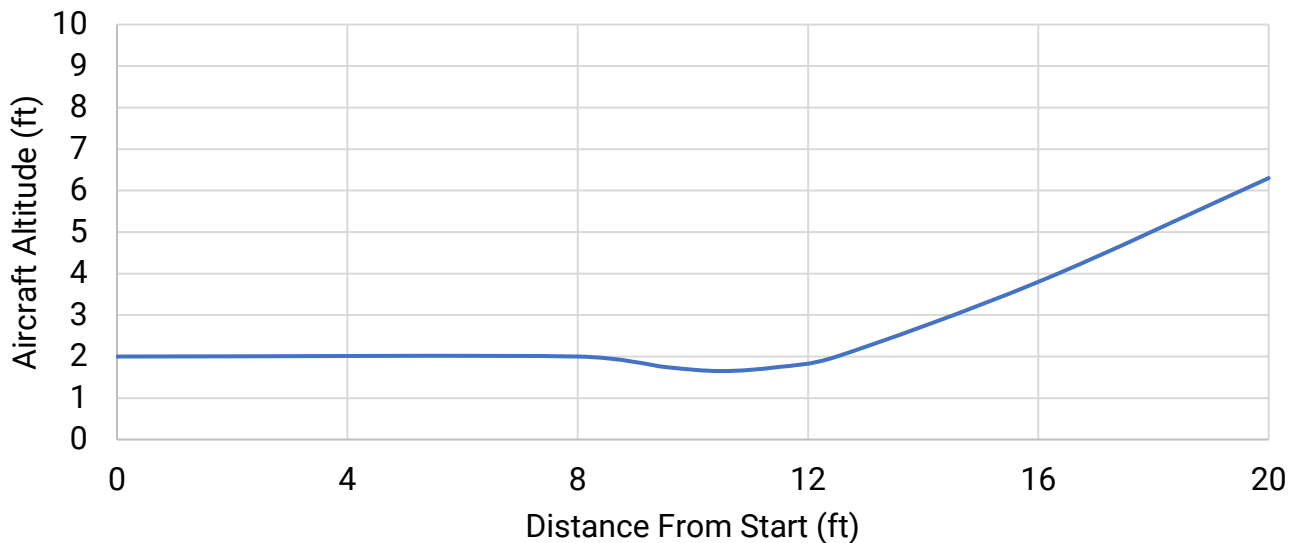
Team Name: *DJS Skylark – MICRO CLASS*

Team Number: *314*

School Name: *Dwarkadas J. Sanghvi College of Engineering*

Time vs Ground Distance

Predicted Time = 7.2s

Altitude vs Ground Distance

AIRCRAFT SUMMARY DATA

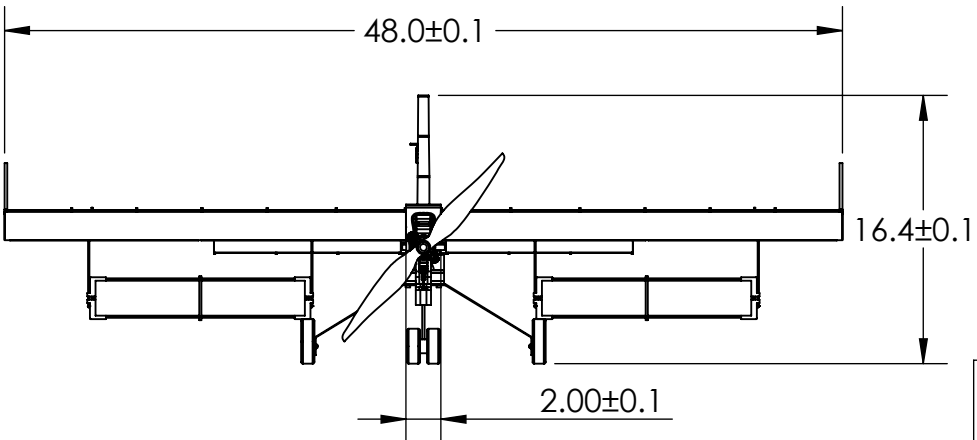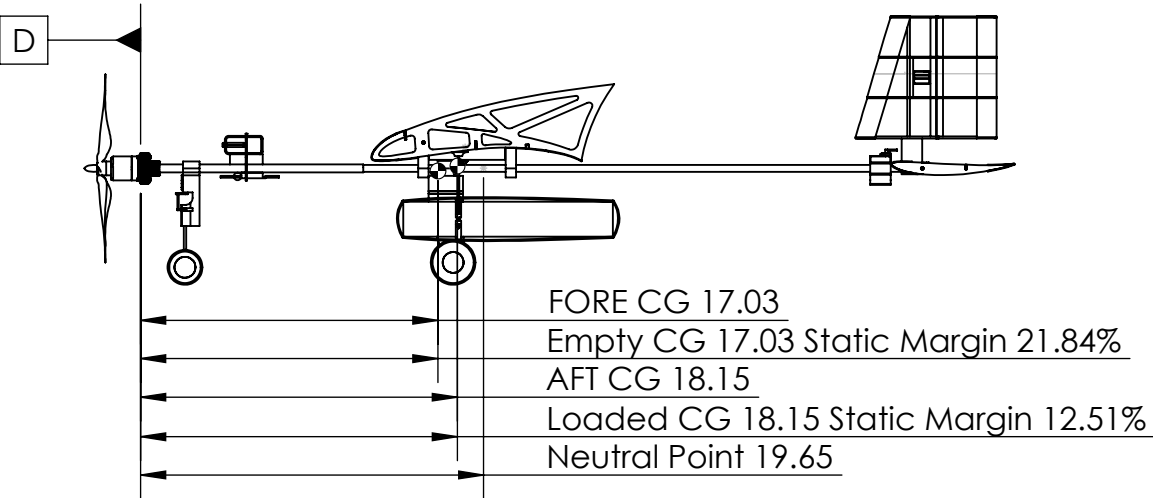| WINGSPAN	MAC	TMA	EMPTY WEIGHT	BATTERY	MOTOR MODEL	MOTOR KV	PROPELLER	SERVO (Nose Landing Gear) (A)	SERVO (Aileron) (B)	SERVO (Elevator) (C)	SERVO (Rudder) (E)
48 ± 0.1"	12"	30 ± 0.1"	2.2 lbs	Dinogy LiPo 850mAh 4S	SunnySky X2820 6 -14 poles	860KV	APC 14x7E	Turnigy 9018-MG (34.72oz-in)	Turnigy 9018-MG (34.72 oz-in)	Turnigy TGY 813 (124.99oz-ln)	Turnigy 9018-MG (34.72 oz-in)

53.3±0.1

MAC: 12.00"

PAYLOAD BAY SECTION

4.36±0.1

1.97±0.1
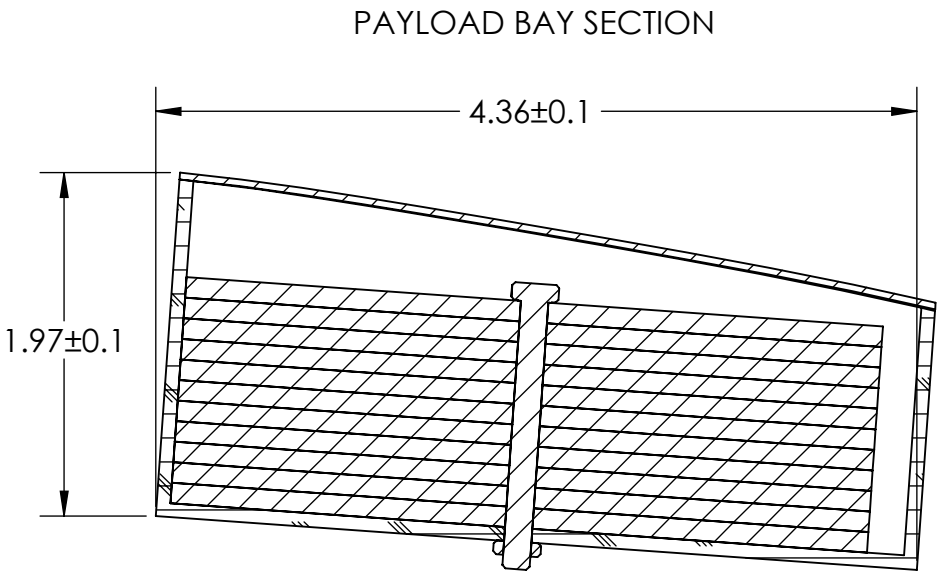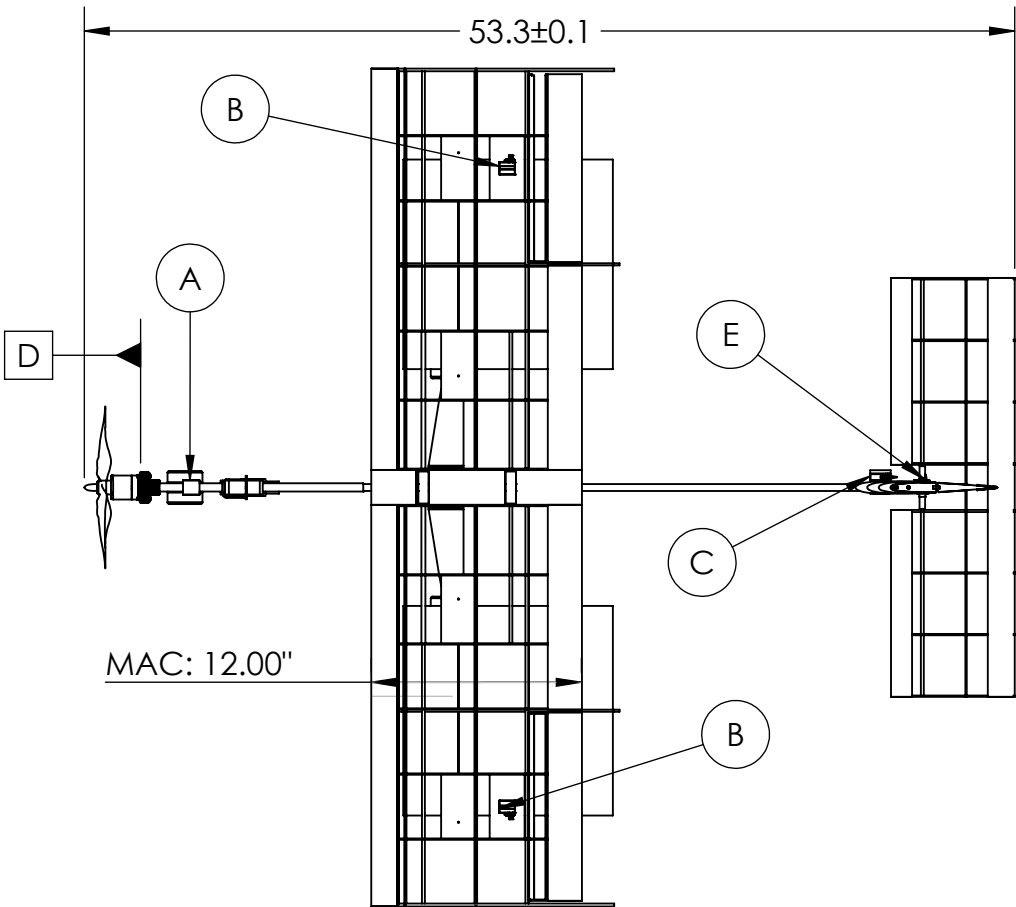
SCALE 1 : 1.1

WEIGHT & BALANCE

SR. NO.	COMPONENTS	WEIGHT (lbs)	ARM (in.)	MOMENT (lbs-in)
1)	MOTOR	0.322	0.889	0.286
2)	BATTERY	0.207	5.899	1.221
3)	PAYLOAD	2.715	18.59	50.47
4)	ELECTRONICS	0.071	6.199	0.441
5)	LARGE BOXES	0.625	21.06	13.16

FORE CG 17.03
Empty CG 17.03 Static Margin 21.84%
AFT CG 18.15
Loaded CG 18.15 Static Margin 12.51%
Neutral Point 19.65

48.0±0.1

16.4±0.1

2.00±0.1

BASIC DIMENSIONS

LENGTH	53.3 ± 0.1"
WIDTH	48 ± 0.1"
HEIGHT	16.4 ± 0.1"

Team NO: 314
Team Name: DJS Skylark - MICRO CLASS

School Name: Dwarkadas J. Sanghvi College of Engineering

SAE Aero Design Knowledge 2021

Size: B   Scale: 1:11   Unit: inches